ACIBADEM MEHMET ALI AYDINLAR UNIVERSITY
INSTITUTE OF NATURAL AND APPLIED SCIENCES

CARVACROL-LOADED HYBRID HYDOGEL SCAFFOLDS AS POTENTIAL WOUND HEALING PATCHES

EYLEM ÖZGE SAVAŞ

M.Sc. THESIS

DEPARTMENT OF BIOMEDICAL ENGINEERING

SUPERVISOR
Assoc. Prof. Özgül Gök Özatay

ISTANBUL-2025

ACIBADEM MEHMET ALI AYDINLAR UNIVERSITY
INSTITUTE OF NATURAL AND APPLIED SCIENCES

CARVACROL-LOADED HYBRID HYDOGEL SCAFFOLDS AS POTENTIAL WOUND HEALING PATCHES

EYLEM ÖZGE SAVAŞ

M.Sc. THESIS

DEPARTMENT OF BIOMEDICAL ENGINEERING

SUPERVISOR
Assoc. Prof. Özgül Gök Özatay

ISTANBUL-2025

DECLARATION

I declare that this thesis work is my own work, I had no unethical behavior at any stages from the planning to the writing of the thesis, I obtained all the information in this thesis in accordance with academic and ethicel rules, I cited all the information and comments that were not obtained with this thesis work, and I provided resources in the list of references. I also declare that there was no violation of any patents and copyrights during the study and writing of this thesis.

06.01.2025
Eylem Özge Savaş
(Signature)

PREFACE AND ACKNOWLEDGEMENT

Firstly, I would like to extend my endless thanks to my advisor Assoc. Prof. Dr. Özgül Gök Özatay, who guided and guided me during this thesis process and provided excellent opportunities for me to realize this thesis. She patiently shared her valuable knowledge and experience with me and made a great contribution not only to my academic but also to my personal development.

I would like to thank the researchers and staff of GÖK Research Group and Biomaterials Center, especially MSc İlayda Güneş and PhD Şeyma Işık, who supported me in laboratory studies during my research, did not let me give up and supported me to get to the best point.

I would like to take this opportunity to express my gratitude and appreciation to Gazi Mustafa Kemal Atatürk, the founder of the Republic of Turkey, who provided us with a modern, scientific and free educational environment and inspired us to progress in every field. His words “En hakiki mürşit ilimdir.” have been my guiding light while conducting this study.

My biggest thank you is to my beloved family, who has always been by my side and has given me strength with their presence. I would like to express my endless love and gratitude to my dear family, who have supported me in all the difficulties I have faced throughout my life and who are the true architects of my success. I would especially like to thank my sister Ekin Gözde Savaş, my inspiration and life energy.

Finally, I would like to thank the scientists and all my colleagues in academia who inspired my work in this thesis. Their knowledge and efforts have always been a light for me.

I hope that this study will contribute to the scientific literature and inspire future research.

TABLE OF CONTENTS

LIST OF ABBREVIATIONS

AB	Acetate Buffer
ACN	Acetonitrile
AV	Aloe Vera
CA	Carvacrol
Ch	Chitosan
DMSO	Dimethyl Sulfoxide
ECM	Extracellular Matrix
EDCI	1-Ethyl-3-(3dimethylaminoproply) carbodiimide
Et_3N	Triethylamine
FT-IR	Fourier Transform-Near Infrared Spectroscopy
GPC	Gel Permeation Chromatography
HA	Hyaluronic Acid
HAp	Hydroxyapatite
LC/MSMS	Liquid Chromatography Mass Spectrometry
mPEG	Methoxy Polyethylene Glycol
mwt	Molecular weight
NaOH	Sodiumhydroxide
NHS	N-Hyroxysuccinimide
NMR	Nuclear Magnetic Resonance Spectroscopy
PBS	Phosphate Buffer Saline
PEG	Poly(ethylene glycol)
PEGDGE	Poly(ethyleneglycol) diglycidylether
SEM	Scanning Electron Microscopy
UV	UltraViole
wt	Weight

LIST OF FIGURES

LIST OF TABLES

ABSTRACT

Carvacrol-loaded Hybrid Hydrogel Scaffolds as Potential Wound Healing Patches

In this thesis study, it was aimed to prepare a drug delivery system for dermal administration, which is composed of natural origin carvacrol encapsulated in composite hydrogel. For this purpose, synthetic poly(ethylene glycol) (PEG) polymer (2 and 5 kDa), was conjugated to the side branches of natural polymer, chitosan. Composite hydrogels were prepared through crosslinking the PEGylated chitosan polymers from the free amine groups on the side branches by using poly(ethyleneglycol) diglycidylether (PEGDGE) (500 Da) as crosslinking agent which contains epoxy functional groups at both ends. The crosslinked hydrogels were characterized for their physical, chemical, mechanical and morphological properties. Then, in order to provide mechanical support to the hydrogel structure, natural hyaluronic acid or aloe vera was added. In addition, carvacrol was encapsulated into the hydrogels to enhance therapeutic effect. In conclude, slow and sustained release properties of bioactive agents in the designed hydrogels offer a great potential therapeutic approach in or wound healing process.

Keywords: Aloe vera, Carvacrol, Drug Delivery Systems, Hyaluronic acid, Hydrogel.

ÖZET

Potansiyel Yara İyileşme Bandı olarak Karvakrol Yüklü Hibrit Hidrojeller Skaffold Tasarım

Bu tez çalışmasında, kompozit hidrojel içerisinde kapsüllenmiş doğal kaynaklı karvakrolden oluşan dermal uygulama için bir ilaç taşıyıcı sistem hazırlanması amaçlanmıştır. Bu amaçla, sentetik poli(etilen glikol) (PEG) polimeri (2 ve 5 kDa), doğal polimer olan kitosanın yan dallarına konjuge edilmiştir. Kompozit hidrojeller, her iki ucunda epoksi fonksiyonel grupları içeren çapraz bağlama ajanı olarak poli(etilenglikol) diglisidileter (PEGDGE) (500 Da) kullanılarak yan dallardaki serbest amin gruplarından PEG'lenmiş kitosan polimerlerinin çapraz bağlanmasıyla hazırlanmıştır. Çapraz bağlanmış hidrojeller fiziksel, kimyasal, mekanik ve morfolojik özellikleri açısından karakterize edilmiştir. Daha sonra hidrojel yapısına mekanik destek sağlamak amacıyla doğal hyaluronik asit veya aloe vera eklenmiştir. Ayrıca, terapötik etkiyi arttırmak için hidrojellerin içine karvakrol enkapsüle edilmiştir. Sonuç olarak, tasarlanan hidrojellerdeki biyoaktif ajanların yavaş ve sürekli salınım özellikleri, yara iyileşmesi sürecinde büyük bir potansiyel terapötik yaklaşım sunmaktadır.

Anahtar Sözcükler: Aloe vera, Hyaluronik asit, Hidrojel, İlaç Taşıma Sistemleri, Karvakrol.

1 INTRODUCTION and AIM

Wound healing is a complex process and is the result of the interaction of various biological and chemical processes. Development of innovative treatment methods to enhance wound healing, prevent infections, and support tissue repair is growing demand. Hydrogels are water-absorbed polymers that emerge in biomaterials field, and are promising tools in wound healing due to their high-water retention capacity, biocompatibility, and biodegradability. Hydrogels composed of both natural and synthetic polymers can improve wound healing processes by providing controlled and sustained release of therapeutics.

Chitosan is a natural polymer commonly used in wound treatment due to its biocompatibility and biodegradability. It reduces the risk of infection in the wound area due to its anti-microbial and homeostatic properties, and allows for faster healing. On the other hand, synthetic polymers such as Poly (ethylene glycol) (PEG) are important for being compatible with physiological environments and providing mechanical strength and flexibility. Moreover, addition of natural compounds like carvacrol, which has anti-inflammatory and anti-bacterial properties, can improve wound healing capacity of the hydrogel-based drug release systems.

The aim of this study is to develop a hydrogel-based drug delivery system that can serve as potential wound healing dress. These hydrogels were synthesized by conjugating natural chitosan with different molecular weights of PEG polymers. Chitosan-PEG conjugates were stabilized using an epoxy-bearing PEGDGE crosslinking agent to obtain hydrogels with different PEGylation degrees. The physical, chemical, mechanical, and morphological characteristics of the obtained hydrogels were evaluated to determine the most suitable hydrogel formulation. M properties of the selected hydrogels were enhanced by addition of natural components such as hyaluronic acid and aloe vera. Finally, carvacrol were encapsulated into these hydrogel structures to design a system that provides controlled and sustained drug release. This thesis study aimed to develop the hydrogel structures with improved mechanical, physical, chemical

and drug release properties to be used as a potential treatment modality for wound healing.

2 BACKGROUND

2.1 Hydrogels

Hydrogels are water-absorbed polymers formed by the formation of cross-links between hydrophilic polymers. Biocompatibility and non-toxicity are main characterises quality of it, like other biomaterials. (1) There are hydrogels in human live for approximately 70 years. (2) Medical, cosmetics and agriculture sectors are hydrogel general application area. Swelling without changing their chemical properties is the main reason for their use in these areas. The use of hydrogels in the medical field is exemplified by their ability to keep contact lenses wettability and gradually release medication. (3) Traditional hydrogels do not affect from environment like changing temperature, pH. (4) However, new generation smart hydrogel change their chemical and physical quality depend on changing environment. (5) Therefore, these structures could be more specific for problematic area. For example, in spinal cord injuries, the temperature of the spinal cord area rises to around 40 ^{o}C, and when heat-sensitive hydrogels are injected there, the drugs in the hydrogels are released only depending on the temperature change in that area. (6)

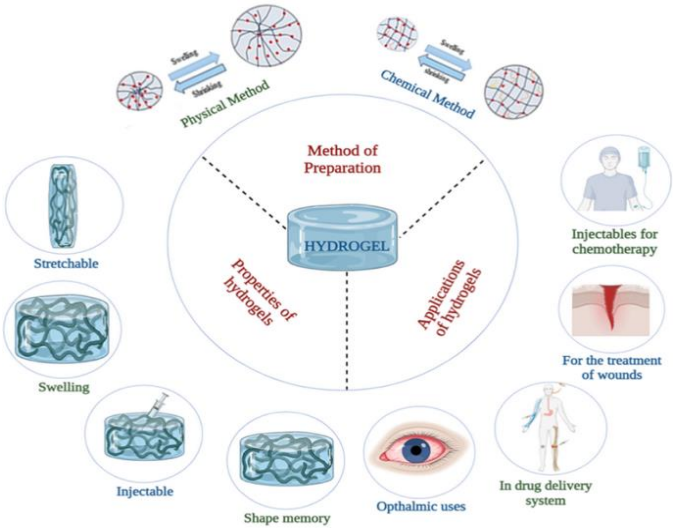

Figure 2.1 Hydrogel preparation methods, properties, and applications overview (7)

2.2 Hydrogel Properties

Hydrogels are three-dimensional hydrophilic polymeric networks. Hydrogels can vary due to raw materials and cross linkers. (8) Each of these chemical, physical and morphological properties plays an important role in the applications of hydrogels in various fields, especially in biomedicine, drug delivery and tissue engineering.

The ability of hydrogels to swell in water-based environments is one of their most important physical characteristics. Swelling varies depending on the hydrogel, the type of crosslinking, the chemical nature of the crosslinking agents and whether the polymer chains are of natural or synthetic origin. For instance, a hydrogel with lower crosslinking density will typically swell more because the polymer chains show greater mobility, allowing them to absorb water more. (9) On the other hand, high crosslinking density can decrease the swelling capacity, stimulating a more solid-like structure. Such swelling behaviour is paramount to drug delivery applications, where the release rate of therapeutic agents can be controlled by tuning the balance between swelling and mechanical integrity. (10)

Biocompatibility is an important property for hydrogels used in medical applications. Ideal hydrogels should support cell attachment and proliferation while minimizing adverse immune responses. The chemical composition and surface characteristics of hydrogels can be tailored to improve biocompatibility. Additionally, hydrogels resemble the extracellular matrix due to their 3D structure. Thanks to this similarity, hydrogels desire in regenerative medicine. Bone and wound repair are among the primary applications of tissue regeneration. In the studies by Sadat-Shojai et al, hydrogels containing HAp and collagen material were implanted into the fractured bone site and the hydrogels acted as an ECM and accelerated the healing process. (11) In the wound healing process, hydrogels can contain gelatine and cellulose and these materials help to promote cell proliferation and antibacterial ability. (12)

Biodegradable structures are defined as materials that can degrade naturally without the need for surgical intervention and without causing any harm in their

environment. (13) Biodegradable hydrogels can exhibit different degradation rates and sensitivity to various environmental stimuli like ion, light, UV, thanks to their chemical composition and structural properties. These properties enable them to have the capacity to release drugs or growth factors in a controlled manner over time. (14) Thus, they can offer high efficacy in biomedical applications by providing an effective release of drugs or molecules for the desired period during the treatment process.

The physical and mechanical properties of hydrogels, particularly tensile strength, elasticity, and toughness, determine their ability to transport payloads such as drugs or hormones. These properties are essential for the sustainability and efficiency of hydrogels in various applications. Due to the 3D interconnected polymer networks, hydrogels exhibit both viscous and elastic properties, influenced by how solvents interact with polymer chains. (13) This viscoelasticity allows hydrogels to deform under mechanical stress while maintaining their original shape. The mechanical strength of hydrogels, such as tensile and compressive strength, is strongly influenced by the degree of crosslinking, which governs polymer chain mobility. The denser the crosslinking, the stronger and less flexible the hydrogel becomes. As a result, hydrogels can exhibit elastic behavior under force and regain load-bearing capabilities, making them suitable for tissue engineering where mechanical performance is critical. The combination of elastic and viscoelastic behavior ensures continuous mechanical stability and flexibility under cyclic or steady stress, making them valuable in various applications.

2.3 Materials in Hydrogel Preparation

The main material of hydrogels is polymeric structures, which can be further divided into natural and synthetic ones. Natural hydrogels are derived from polysaccharides, proteins, and other biopolymers. Conversely, synthetic hydrogels are made in laboratory environment.

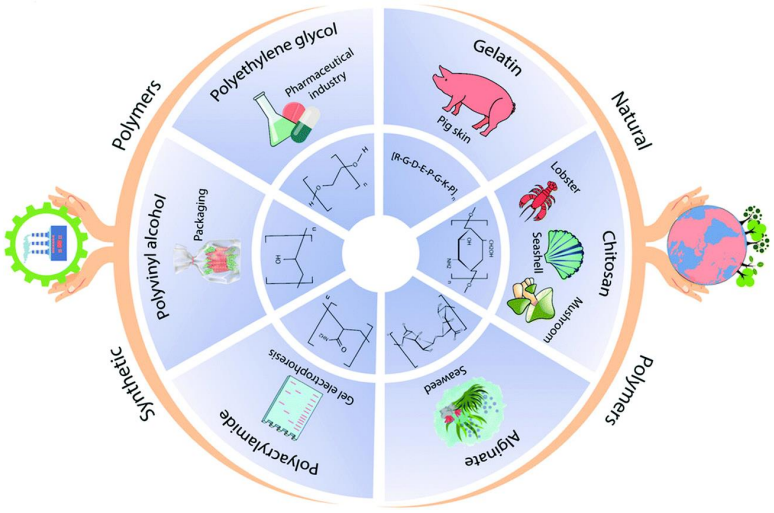

Figure 2.2 Schematic illustration of natural and synthetic polymers (15)

2.3.1 Synthetic Polymers

Synthetic polymer made in laboratory. Poly(ethylene glycol) (PEG) and polyacrylamide are typical exam of it. These materials allow precise control over the properties of the hydrogel, such as swelling behaviour, mechanical strength, through tuning the crosslinking density and slow degradation rate. (16) Furthermore, synthetically derived polymers can be manufactured with a level of purity and uniformity that is not always possible with naturally occurring polymers. For applications such as drug delivery, these conditions need to be met for predictable and reproducible delivery profiles. (17) The most important disadvantages of these structures are the potential lack of bioactivity (which may lead to poor cell attachment and proliferation) and the environmental impacts associated with the production and disposal of synthetic polymers. (18)

2.3.1.1 Poly (ethylene glycol) (PEG)

Poly(ethylene glycol) (PEG) is a non-toxic, non-antigenic, and non-immunogenic linear or branched synthetic hydrophilic and biodegradable polymer. (19) Its molecular weight can range from 200 Da to 7000 Da, giving it various physical and chemical properties. PEG-based hydrogels are used in wound models because they

enable the proliferation and development of cells on the injured surface, thus accelerating the healing process. In the research conducted by Chen et al., PEG-based hydrogels were applied to cuts in Sprague Dawley rats, and it was observed that bleeding was halted, and incision openings closed within just a few minutes. This highlights the potential of PEG hydrogels in wound healing applications due to their rapid hemostatic and adhesive properties, which allow them to facilitate tissue repair effectively. (20) The results suggest that PEG-based hydrogels could be highly beneficial in surgical or injury-related scenarios by providing quick and efficient wound closure process.

2.3.2 Natural Polymers

Natural polymers come from nature like plant, animal. While starch and alginate are example natural polymer from plant, chitosan and gelatine are example of natural polymer from animals. (21) Alteration or functionalization of natural polymers is easily performed since there are numerous reactive groups in their structure like carboxylic acid (-COOH), amine ($-NH_2$), and hydroxyl (-OH) groups are plenty. (12) They generally show very good biocompatibility, biodegradability, gel-forming ability, low toxic and environment friendly. However, weakness of mechanical features, rapid degradation rate, poor antioxidant properties, and undesirable stimuli responsive nature are drawbacks of natural polymers. (12, 21)

2.3.2.1 Chitosan

Chitosan is a polymer of chitin, which constitutes the exoskeleton of arthropods. Chitosan is a biocompatible, biodegradable, and antimicrobial polysaccharide that possesses structural similarities to glycosaminoglycans found in the extracellular matrix (ECM). (22, 23) The molecular weight and deacetylation level of chitosan are directly related to its physical and mechanical properties. The mechanism by which chitosan facilitates wound healing involves several biological processes. One of the earliest processes that kick in for wound healing is hemostasis, and the literature reveals that chitosan-based formulations have been shown to induce this phenomenon. Blood clot formation is promoted, and bleeding is reduced through platelet recruitment and

activation. Ishihara et al. observed approximately 50% of wound closure along with contraction during the initial phase (within 2 days) in wound models prepared with chitosan-based hydrogels. (24)

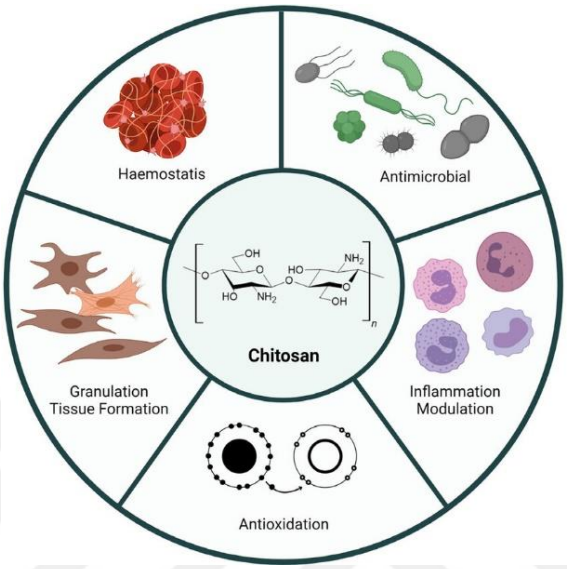

Figure 2.3 Key biological functions of chitosan in wound healing (25)

Formation hydrogel ability of chitosan prevents the evolution of hydrogels that support tissue repair and regeneration by keeping wounds wettability for quicker healing. Chitosan's hydrophilic nature extends its ability to absorb and maintain wound exudate, thus avoiding maceration and aiding wound healing. Moreover, chitosan promotes healing not only through its physical but also biological characteristics. Studies have confirmed that chitosan participates in tissue regeneration by promoting the proliferation of cells such as fibroblasts and keratinocytes. N-acetyl-D-glucosamine in chitosan structure reduces the healing times because this molecule is quickly absorbed by tissues. (26) Research by Hao et al. revealed that the chitosan-based hydrogel exhibited a swelling rate of 132% at 37 °C, which allowed the hydrogel to regulate the moisture level in the lesion by absorbing tissue fluids. In studies in mice with diabetes, the hydrogel was observed to rapidly adhere to the wound, stopping bleeding and providing a favorable environment for healing, a process that led to 99% wound healing within 14 days. (27)

One of the disadvantages associated with chitosan is its insufficient mechanical strength, difficulties in the production of fibrous wound dressings, in addition to the fact that this material is highly sensitive to external factors such as pH and temperature due to the hydroxyl and amino groups present in its chemical structure. These difficulties can be minimized by the use of cross-linkers such as glutaraldehyde, genipin or conjugated with synthetic polymer such as PEG.

2.3.2.2 Hyaluronic Acid (HA)

Hyaluronic acid (HA), a naturally occurring polysaccharide, aids in various stages of the wound healing process. Its ability to retain wettability environment, promote cell migration and modulate inflammatory responses is a factor in wound healing.

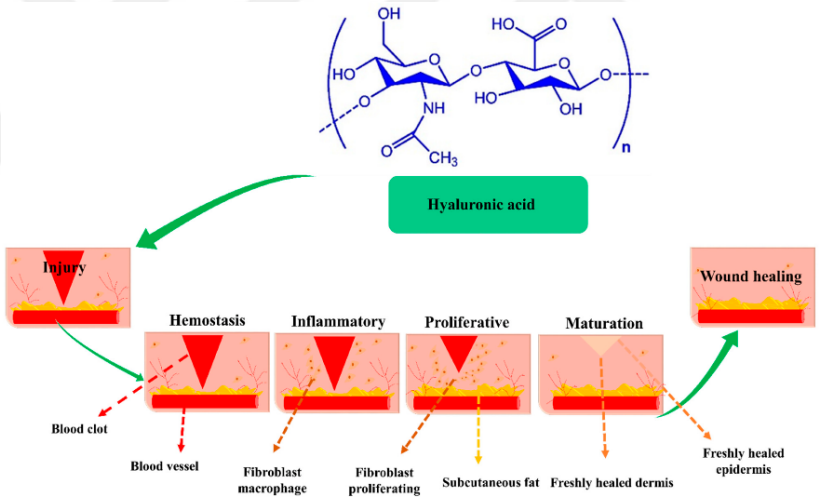

Figure 2.4 Hyaluronic acid effect during wound healing process (28)

The role of HA in wound healing begins in the early stages of what, particularly during homeostasis when it accumulates earlier than platelets. It is this accumulation that it helps to adjust the mechanical properties of the crust and mediates the migration of cells to the wound site, which is essential for subsequent healing processes. (29, 30) Furthermore, HA has been shown to increase the adhesion and growth of fibroblasts, which are key players in the wound healing process, thereby accelerating tissue repair.

HA polymer creates suitable environment for wound healing treatment. It enriches the migration and proliferation of various cell types such fibroblasts and keratinocytes that are crucial for the formation of granulation tissue and re-epithelialization during the healing process. (31) Its presence in the ECM maintains hydration and provides structural support. This ensures proper functioning of healing tissues. As a literature example, the effect of HA on chronic leg ulcer wounds was investigated in a randomized study by Humbert et al. As a result of these studies, it was observed that wound healing process shortened down to 45 days, with the number of injured individuals decreased from 31,1% to 9,3%, which also and decreased from 37,8% to 16,3% in at the end of 60 days. (32)

HA polymers play a significant role in modulating inflammatory response during wound healing. It effects the production of several cytokines and growth factors that are critical for the inflammatory phase of healing. (32)

2.3.2.3 Aloe Vera (AV)

Aloe vera promotes wound healing by several mechanisms. In fact, studies found that treatment with Aloe vera greatly enhances collagen synthesis (an essential component of wound repair) and fibroplasia (the formation of fibrous tissue during healing), which in turn results in a reduced size of the wound. Tariq et al. proved that Aloe vera hydrogels healed the wounds with 98.33% contraction in 13 days in wound models created in albino diabetic rats. (33) Wound healing is also supported by the antimicrobial properties of Aloe vera. Saponins provide a natural cleanser and antiseptic action that impedes microbial development around the wound, hence reducing the probability of infection. (34) This may produce an aseptic milieu, which encourages the proliferation of fibroblasts and, later on, supports the development of granulation tissue, enabling the proper healing process to occur. (35)

AV contains various chemical components that are affect tissue regeneration biologically. (36) For example, C and E vitamin that relate antioxidant features, in AV.

These components reduce oxidative stress and create more suitable regenerative environment. (37)

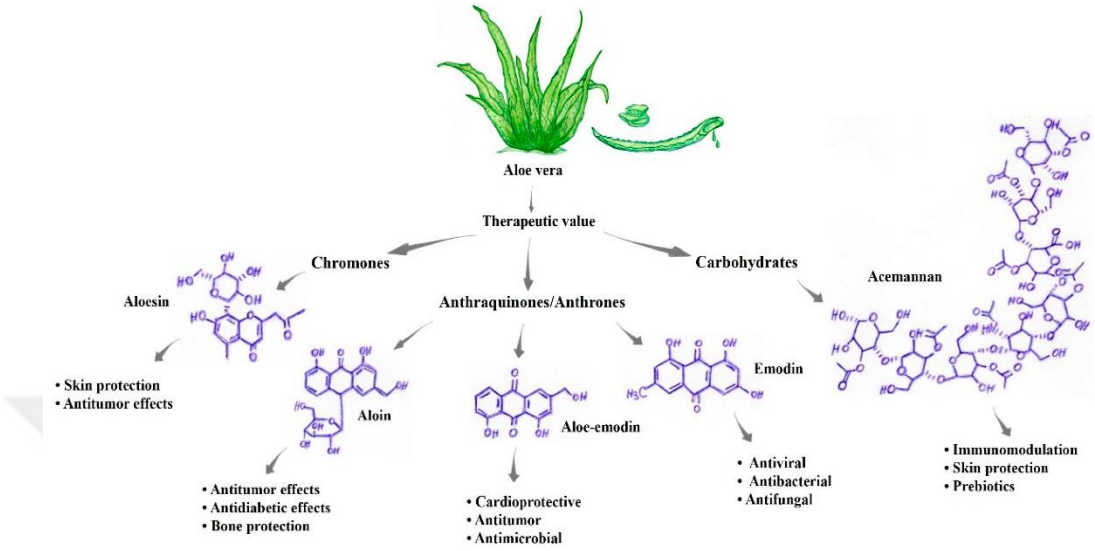

Figure 2.5 Therapeutic value of aloe vera: bioactive compounds and their effects (38)

2.3.3 Hybrid Hydrogels

Hybrid hydrogel is a class of materials created by combining two or more different types of polymers, often providing enhanced properties compared to their individual forms. (8) These structures, which are usually formed by combining a natural and a synthetic polymer, incorporate the advantageous properties of both sides while eliminating their negative properties. (39) This situation results in more durable structures with high biocompatibility.

2.4 Crosslinking Strategies

Crosslinking of natural or synthetic polymers leads to a network of 3D structures. (40) Crosslinking level influence the physical properties of the hydrogel, such as elasticity, degradation rate, and permeability to dissolved substances. In hydrogels, crosslinking can be divided into two general categories: chemical (covalent) and physical (non-covalent). (40)

Physical crosslinking process relies on non-covalent interactions such as physical entanglement of polymer chains, hydrogen bonding, ionic interactions, or hydrophobic effects; these can be reversible and allow for dynamic changes in the hydrogel structure. (8) These bonds can vary depending on environmental conditions as well. The absence of non-toxic crosslinking agents is the main feature of this type of crosslinking process. (8)

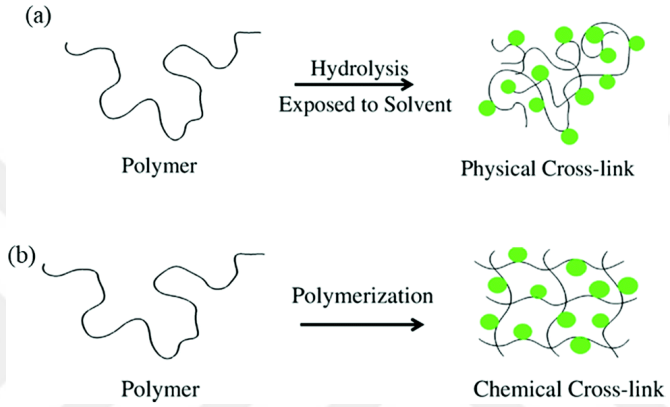

Figure 2.6 Schematic illustration of physical and chemical cross-link (a- Physical crosslinking b- Chemical crosslinking) (15)

Chemical crosslinking involves covalent bonding between polymer molecules themselves or between two different polymer chains, facilitated by assisting molecules, hence more stable and lasting attachment to the environment. (8, 40) Covalent bonds primarily form between the functional groups of polymers (-OH, -COOH, -NH_2), that are responsible for enhancing the hydrophilicity of water-soluble polymers. (41)

2.4.1 Epoxy Based Crosslinking

Epoxy-based crosslinkers react with hydroxyl groups present in the polysaccharides or other polymer matrices, thus allowing chemical cross-linking to happen and a stable three-dimensional network to form. (42) The versatility of epoxy-based crosslinkers, examples of which include epichlorohydrin (ECH) and glycidyl methacrylate (GMA), has enabled the synthesis of hybrid hydrogels, further enhancing their structural integrity and functionality. So, the presence of epoxy groups allows for

preparing hydrogels of tunable properties, including sensitivity to environmental stimuli. (43) The crosslinking agents containing the epoxy ring are highly reactive since the oxygenated three-membered ring opens immediately upon contact with a nucleophile. The opening of this so-called oxirane ring creates a highly reactive intermediate, usually an alcohol. During the opening of the epoxide ring, the nucleophilic group of the polymer or biomolecule forms a covalent linkage with an active epoxide species. This can occur between chains from different polymers or between a polymer and a biomolecule, leading to cross-linking. (44) Hydrogels obtained by this cross-linking mechanism were shown to exhibited improved mechanical properties, swelling behavior and biocompatibility making them suitable scaffolds for drug delivery and tissue engineering applications.

2.4.1.1 Poly (ethylene glycol) diglycidyl ether (PEGDGE)

Poly (ethylene glycol) diglycidly ether (PEGDGE) is a water soluble crosslinker agent which has two epoxy groups at both ends. (45) These groups assist the covalent bonds creation formation among various polymer chains which has hydroxyl and amine groups, hence creating a 3D dimensional network that is required for hydrogels. The content of the PEGDGE segment can be adjusted through its ratio for crosslinking step in order to adjust the crosslinking density and mechanical strength of the hydrogel. (46, 47) Moreover, the presence of epoxy groups allows for further functionalization by incorporating bioactive molecules or other polymers into the hydrogel matrix, thereby ensuring biocompatibility and recoverability. (48)

There are many different molecular weights in PEGDGE. However, the one with a molecular weight of 500 Da weight has shown several advantages compared to other molecular weights. One of them is the ideal stability, flexibility and mechanical strength. For example, the viscoelastic properties of hydrogels can be fine-tuned by adjusting the molecular weight of the cross linker, and 500 Da generally gives the best performance in terms of both elasticity and strength. (49) Another feature is that PEGDGE 500 Da exhibits favorable thermal stability properties, which are essential to maintain the integrity of the material during processing and application. Finally and most

importantly, PEGDGE 500 Da has low toxicity profile, which is particularly important in its biomedical applications. (50)

2.5 Application of Hydrogels

Hydrogels are used in many fields in the medical sector due to their high mechanical strength, adjustable chemical properties and high water retention capacity. Some applications include tissue engineering, drug delivery systems, regenerative medicine, contact lenses, cosmetics and diagnostic applications such as diagnostic kits and biosensors. Thanks to their ECM-like structure, hydrogels can act as scaffolds to facilitate cell growth, attachment and proliferation. (13) The wettability and cell growth accelerates the wound healing process.

2.5.1 Hydrogels as Wound Healing Scaffolds

Throughout their lives, people struggle with many physical, thermal, chemical or chronic injuries. The process of wound healing represents a multi-layered process that includes haemostasis, inflammatory, proliferative and maturation/remodelling phase. (51) Hydrogels are involved in the field of wound healing as effective scaffolds that facilitate tissue regeneration and repair. One of the primary advantages of hydrogels in wound healing is to provide a protective barrier against pathogens In the chitosan/dextran-based hydrogel studies conducted by Du et al., chitosan/dextran-based hydrogels exhibited antimicrobial activity against Pseudomonas aeruginosa and Staphylococcus aureus bacterial species, which are commonly encountered in the wound healing process and delay the healing process, with 96.4% and 95.0% termination efficiency, respectively. (22)

Wound dressings can help accelerate the healing process and protect the wound, yet conventional dressings such as gauze, cotton, and bandages must be changed frequently, as they struggle to provide a wettability environment necessary for proper healing. (13) Hydrogels with high water up take capacity can be used as an effective platform to overcome the shortcomings of this traditional method. Scaffolds from it can be designed to have bioactive properties that promote angiogenesis, a critical process in

wound healing that enables new blood vessels to form. Studies by Kim et al. confirmed that hydrogels infused with bioactive factors have a significant positive effect on angiogenic responses and increase tissue perfusion and oxygenation at the wound site. (52)

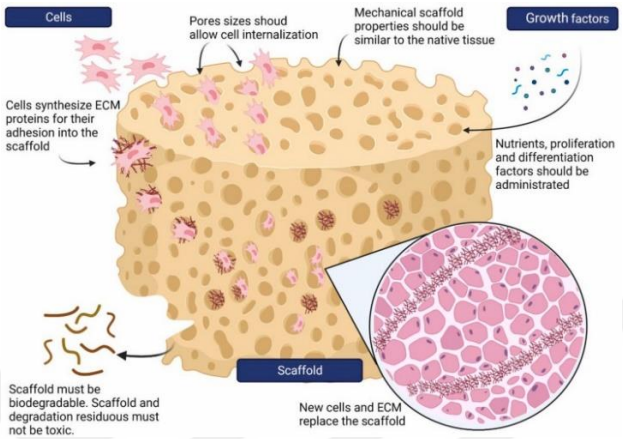

Figure 2.7 Cellular interaction and scaffold integration (51)

2.5.2 Hydrogels as Drug Delivery Systems

Drug delivery systems (DDS) are one of the biotechnological methods that enable effective and controlled delivery of a drug to targeted areas in the body. Thanks to this method, drug treatment can be applied to problematic areas at the desired dose and over a long period of time, thus minimizing side effects with maximum bioavailability. DDSs are used especially in cancer treatment to limit the spread of drugs throughout the body and ensure that they reach only cancerous cells. Although there are many methods such as nanoparticles and liposomes, hydrogels are the most widely used method for this system. With unique properties such as flexibility, hydrophobicity and biocompatibility, hydrogels emerge as very effective scaffolds as drug carriers. Being three-dimensional networks of hydrophilic polymers, hydrogels absorbs high amounts of water and instantly anchor to the desired site. (8) Drugs encapsulated into the porous structures of such networks can be liberated in a pre-determined rate at the site of administration in the body. Hydrogels have versatile delivery methods, including oral, dermal (transdermal) and injectable routes.

2.5.2.1 Carvacrol Loaded Hydrogels

Carvacrol, (2-Methyl-5-[1-methyl ethyl]-phenol) abundant in many plants like oregano, thyme, sweet basil and black cumin, is a solution for wound healing therapy. (53) It has the fundamental properties like being anti-inflammatory and antimicrobial effects in these four consecutive phases leading to normal wound healing.

The mechanisms by which carvacrol facilitates wound healing are multifactorial. One of the primary pathways involves the modulation of inflammatory responses. Carvacrol has been shown to inhibit the production of pro-inflammatory cytokines such as interleukin-6 (IL-6) and tumour necrosis factor-alpha (TNF-α), which are important mediators in the inflammatory phase of wound healing. Studies by Hotta et al. in human macrophage-like U937 cells and by Han et al. in bone marrow (BM) cells from C57BL/6 mice showed that carvacrol significantly reduced the expression levels of these cytokines, thereby alleviating excessive inflammation that can impede healing. (54, 55) This anti-inflammatory effect is particularly beneficial in chronic wounds, where prolonged inflammation can lead to delayed healing and an increased risk of infection.

The antimicrobial properties of carvacrol further enhance its therapeutic potential in wound healing. Carvacrol has shown to provide significant activity against a wide range of pathogenic bacteria and fungi, including methicillin-resistant Staphylococcus aureus (MRSA) and Candida species. In the release studies published at Scaffaro et al., carvacrol-loaded electrospun membranes exhibited notable antimicrobial activity for up to 144 hours and reduced biofilm formation in single and mixed cultures of *Staphylococcus aureus* and *Candida albicans* by 92–96% and 88–95%. (56) The ability of carvacrol's ability to inhibit microbial growth not only reduces the risk of infection in wounds, but also promotes the overall healing process by creating a more favourable environment for tissue repair.

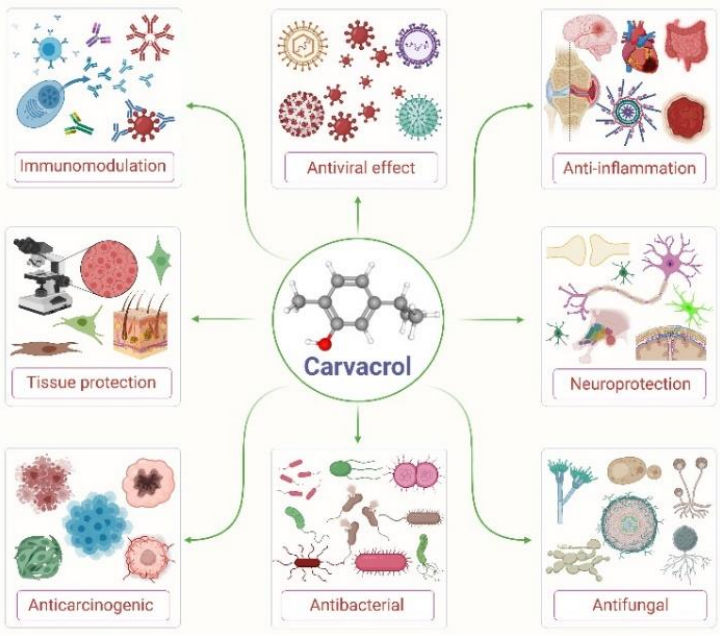

Figure 2.8 Biological activities of carvacrol in tissue protection and disease prevention (57)

The therapeutic potential of carvacrol extends beyond its direct effects on wound healing. Its incorporation into various formulations, such as hydrogels and nanocarriers, is being used to enhance its bioavailability and sustained release at the wound site. These advanced delivery systems can optimize the therapeutic effects of carvacrol, ensuring its prolonged exposure to target tissues and maximizing its beneficial outcomes.

3 MATERIALS AND METHODS

3.1 Materials

Chemical synthesis and purification/analysis: Poly (ethylene glycol) methyl ether (PEG, Mw 2000 Da), Poly(ethylene glycol) methyl ether (PEG, Mw 5000 Da), Triethylamine (Et_3N), succinic anhydrite, Dimethyl sulfoxide (DMSO), anhydrous dichloromethane(CH_2Cl_2), N-Hyroxysuccinimide(NHS), 1-Ethyl-3-(3dimethyl-aminoproply) carbodiimide (EDCI), Chitosan (high molecular weight), Poly(ethyleneglycol) diglycidylether (PEGDGE Mw 500 Da), %2 Acetic Acid solution, Sodium hydroxide (NaOH), Hyaluronic acid (HA), Aloe vera (AV), Carvacrol (purity 98%, Sigma–Aldrich), absolute ethanol (purity >99,5%, Merck) and Tween80 (Sigma–Aldrich) were used.

3.2 Synthesis and characterization of PEGylated Chitosan Conjugates

3.2.1 Carboxylic Acid-Functionalized PEG chains

For the preparation of the hydrogel scaffold, carboxylic acid functional groups were added separately to one end of polyethylene glycol (PEG) chains of molecular weights 2 and 5 kDa. Each of these polymers was obtained in the amount of 1.0 g and dissolved in anhydrous dichloromethane (CH_2Cl_2). These polymers were then stirred for 30 min at room temperature in the presence of 0.75 mol 75.89 mg for 2kDa mPEG and 0.3 mol 30.05 mg triethylamine (Et_3N) for 5 kDa mPEG. Then, 0.75 mol 75.05 g succinic anhydride for 2kDa mPEG and 0.3 mol 30.02 mg succinic anhydride for 5kDa mPEG dissolved in 2 mL dichloromethane were added to the PEG polymer solution, respectively, and the reaction mixture was stirred at 500 rpm overnight. After concentrating the reaction feedstock by rotary evaporator, the polymer was precipitated into cold diethyl ether (100 mL). The precipitated polymer was kept at -20°C and then filtered through a filter paper to obtain as a white solid (0.93 g, 93% for PEG2k-carboxylic acid and 0.91 g, 91% for PEG5k-carboxylic acid).

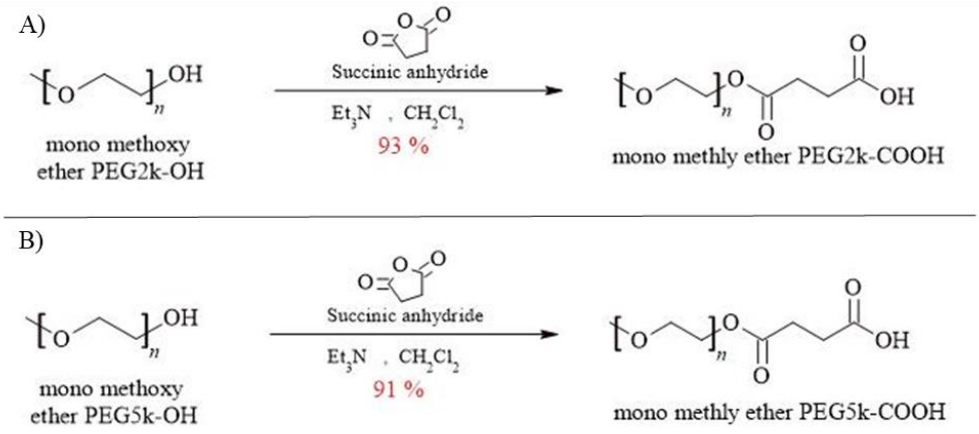

Figure 3.1 Chemical representation conversion of the mPEG form to the PEG-carboxylic acid form (A- conversion of PEG2k, B-conversion of PEG5k)

3.2.2 Attachment of PEG chains to Chitosan

Then, these polymers were dissolved separately in 2 mL of anhydrous DMSO and the carboxylic acid groups at one end were activated using NHS molecules (0.035 mol, 0.4 mg) via EDCI coupling agent under basic conditions (triethylamine, Et_3N). To this solution was added a 1 wt% solution of chitosan (high molecular weight - 0.2 µmol, 100 mg) dissolved in 2% acetic acid solution. This conjugation reaction continued for approximately 18 hours. Following this amidation reaction, the PEG chains are predicted to bind to the amine groups on the side branches of chitosan. Ch-PEG2k conjugate was named as C1 and Ch-PEG5k conjugate was named as C2.

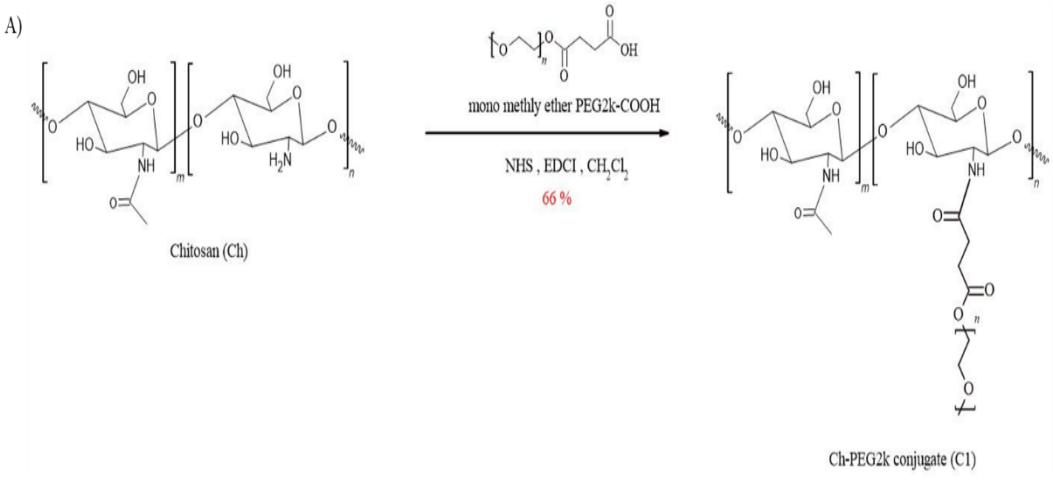

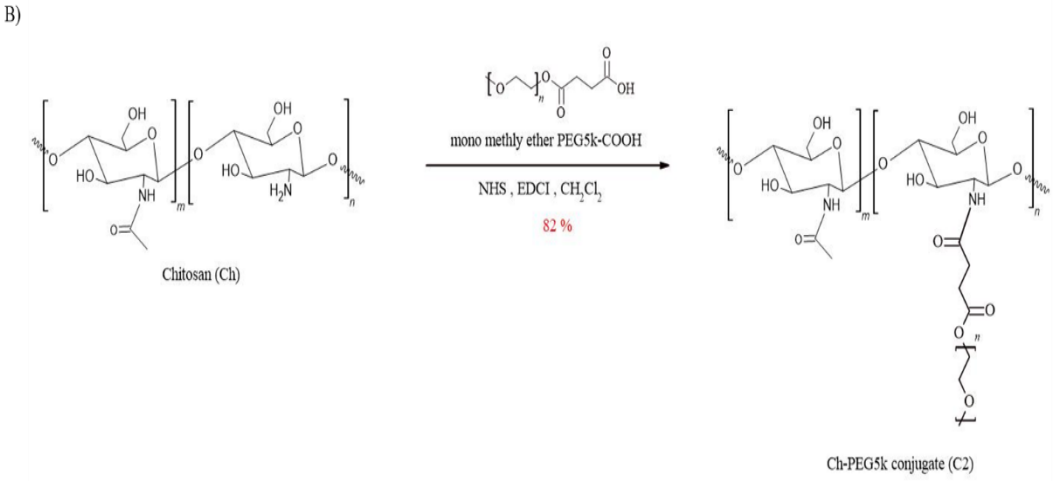

Figure 3.2 Chemical representation of Ch-PEG conjugates from chitosan and PEG-COOH (A- Ch-PEG2k conjugate, B- Ch-PEG5k conjugate)

The resulting mixture was purified by dialysis against ddH_2O (Mwt cut-off: 3500 Da) to obtain chitosan-PEG conjugate in pure form. Then, the conjugates were dried using freeze-dried lyolization (FreeZone Plus 6 Liter Cascade Freeze Dry Systems Model: 7934031). The yields of the obtained solid conjugates were calculated and their chemical characterization was performed using FT-IR and NMR spectroscopies.

The chitosan polymer and its PEGylated conjugate(s) were analysed by a GPC (Gel Permeation Chromatoıgraphy) system for their molecular weight and size distribution. The difference was divided by the molecular weight of PEG used for the conjugation in order to calculate the average number of PEG polymers attached to the side chain of chitosan. TOSOH EcoSEC® GPC system was used with a refractive index detector (RID) and UV detector. Also the system was connected to a Wayyt DAWN Line of Multi-Angle Light Scattering detector (MALZ) with a 18 angle laser system. The samples were prepared at a concentration of XX mg/mL in 2% acetic acid solution and then run in the GPC system with 10 mM PBS as the mobile phase at a flow rate of 1 mL/min. TOSOH TSKgel G3000SWxl 7.8mm LD x 30cm, 5 um column was used as the stationary phase. The results were evaluated using Astra software by obtaining a linear Zimm plot.

Number of PEGs Attached to Chitosan Side Chains = (Mn of conjugates - Mn of Chitosan) / Mwt of PEG (eq1)

Mn = Number Average Molecular Weight

Mwt = molecular weight of PEG

3.3 Hydrogel Preparation and Optimization

Within the scope of the project, the objective is to fabricate biocompatible dermal scaffolds utilizing PEGylated chitosan conjugates, facilitated by a cross-linking agent. Poly(ethyleneglycol) diglycidyl ether (PEGDGE) with a molecular weight of 500 kDa has been selected as the cross-linking agent due to its favourable water solubility, commercial availability, and low toxicity profile.

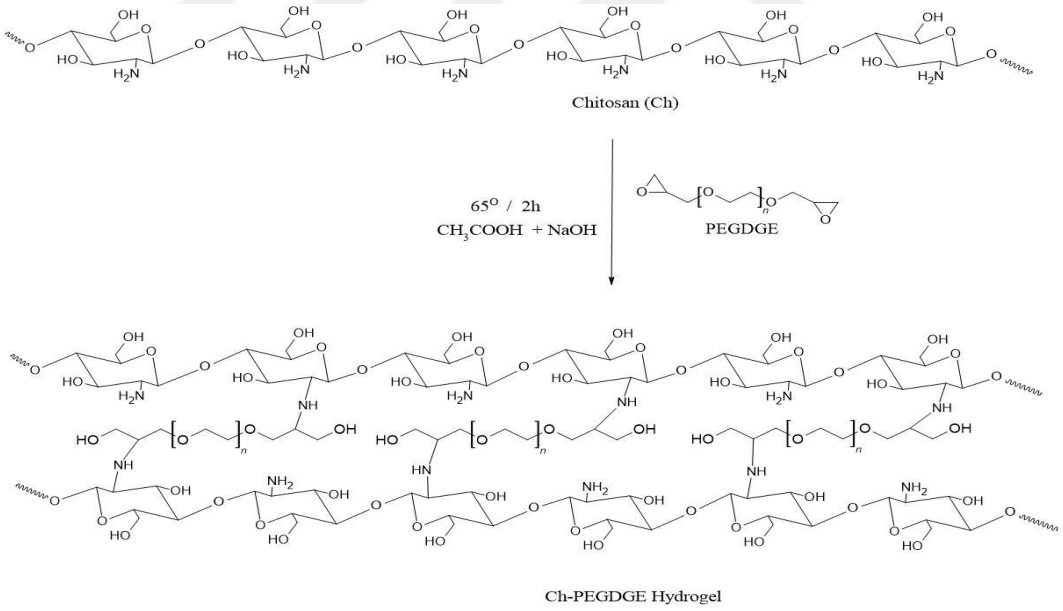

Figure 3.3 Chemical crosslinking of chitosan with PEGDGE

Efforts were directed towards establishing the optimal gelation conditions utilizing the cross-linking agent PEGDGE. Initially, a systematic exploration encompassing temperature variations ranging from 65 ^{o}C to 80 ^{o}C, pH conditions ranging from acidic (pH 3) to neutral (pH 7.4), and diverse volume and weight ratios of

cross-linker (10, 20 and 40 %) were conducted. It was determined that the most efficient gelation was achieved at 65 ºC, under neutral pH conditions, and with the tested volume ratios.

Table 3.1 Experimental Conditions and Variable Parameters in the Hydrogel Optimization Process

No	Code	Component	PEGDGE (%w/v)	PEGDGE (%v/v)	pH	Gelation Temperature	Gelation
1	HG1	Ch	10	-	3	80	-
2	HG2	Ch	20	-	3	80	-
3	HG3	Ch	40	-	3	80	-
4	HG4	Ch	40	-	8	80	-
5	HG5	Ch	40	-	7	80	-
6	HG6	Ch	-	10	7	80	+
7	HG7	Ch	-	20	7	80	+
8	HG8	Ch	-	40	7	80	+
9	HG9	Ch	-	10	7	65	+
10	HG10	Ch	-	20	7	65	+
11	HG 11	Ch	-	40	7	65	+
12	HG 12	C1	-	10	7	65	+
13	HG 13	C1	-	20	7	65	+
14	HG 14	C1	-	40	7	65	+
15	HG 15	C2	-	10	7	65	+
16	HG 16	C2	-	20	7	65	+
17	HG 17	C2	-	40	7	65	+

Chitosan (Ch), Chitosan-PEG2k conjugate (C1) and Chitosan-PEG5k conjugate (C2) were dissolved separately in 100 µL of 2% acetic acid solution at a concentration of one milligram each. To ensure pH neutrality in these solutions, 100 µL of 0.35M NaOH solution was added. Then, 20, 40 and 80 µL of crosslinkers were added to the neutralized solutions separately corresponding to 10, 20 and 40% volumetric ratios, respectively. In total, twelve hydrogels with different compositions and crosslinker ratios were synthesized. These hydrogels were subjected to extensive characterization analyses.

3.4 Characterization of Hydrogels

Hydrogels were evaluated using the characterization methods detailed below:

Determination of Swelling Capacity: Following the formation of hydrogels, to prevent the polymers from dissolving, they were rapidly frozen in a refrigerator at -80 ^{o}C. Subsequently, water was removed using the lyophilisation method, and these hydrogels were incubated in distilled water at a room temperature at specified time intervals. The water taking capacities of the hydrogels over time were calculated by comparing them to their initial dry weights.

$$\text{Water Retention Capacity (\%)} = ((W_t - W_0) / W_0) \times 100 \quad \text{(eq2)}$$

W_t = weights of swollen
W_0 = dried state samples

Morphological Evaluation: The prepared hydrogels were imaged in a Scanning Electron Microscope (SEM) (Leica Quanta 650 FEG). Lyophilized samples were coated with 20 nm gold (Au/Pb) under vacuum and fixed on the stub with carbon tape and observed under high vacuum to visualize the pore structures.

Functional Group Evaluation: The chemical structures of the hydrogels were determined by examining the characteristic functional groups present in the polymers using FT-IR spectroscopy (ThermoScientific NICOLET iS10). This allowed for the measurement of the light absorption capacities of the samples at different wavenumbers.

Determination of Mechanical Properties: The gelled hydrogels were analysed for their mechanical properties using a rheometer (Malvern Kinexus) under 1000 Hz pressure using J2 SR 4703 SS geometry. The degradation property was studied by taking measurements at parameters from = 0.01 to = 1000 and at 25 ^{o}C (51 data points).

3.5 Addition of Hyaluronic acid (HA) or Aloe Vera (AV) into Hydrogels

Based on the results of physical, chemical, and morphological characterizations, as well as water retention analysis, it was determined that the hydrogel formed with C2, cross-linked with PEGDE as a volumetric ratio of 20%, under neutral conditions at 65 °C exhibited the most efficient structure. To further strengthen this hydrogel structure and investigate the impact of natural and synthetic substances on this gel matrix, hyaluronic acid (HA) and aloe vera (AV) were added into hydrogels, separately, at weight ratios of 0.5, 1, and 2%.

3.5.1 Addition of Hyaluronic acid (HA)

Dissolved one milligram of C2 in a solution containing 100 µL of 2% acetic acid and 100 µL of 0.35M NaOH were added to obtain a total volume of 200 µL. Hyaluronic acid (HA) was then added to these solutions at 0.5, 1 and 2% weight ratios corresponding to 1, 2 and 4 mg, respectively. The resulting hydrogels were washed 3 times with ddH_2O and then subjected to mechanical analysis using a rheometer. They were then freeze-dried using lyophilization method to calculate their gel conversion. The dried hydrogels were subjected to chemically analysed using FT-IR spectrometer and morphological evaluation were done using SEM device. Water uptake capacity was determined by weighing the hydrogels upon incubation in water at different time intervals (0, 5, 10 min .....) for 1 hour.

3.5.2 Addition of Aloe Vera (AV)

Dissolved one milligram of C2 in a solution containing 100 µL of 2% acetic acid and 100 µL of 0.35M NaOH were added to obtain a total volume of 200 µL. Aloe vera (AV) was then added to these gels at 0.5, 1 and 2% weight ratios corresponding to 1, 2 and 4 mg, respectively. The resulting hydrogels were washed 3 times with ddH_2O and then subjected to mechanical analysis using a rheometer. Subsequently, they were freeze-dried using the lyophilisation method to calculate their conversion. The dried hydrogels were chemically analysed using an FT-IR spectrometer, and their morphological evaluation were done using SEM. Water uptake capacity was determined

by weighing the hydrogels upon incubation in water at different time intervals (0, 5, 10 min .....) for 1 hour.

Table 3.2 Addition of Hyaluronic acid (HA) or Aloe Vera (AV) into Hydrogels

No	Code	Component	PEGDEGE (% v/v)	HA (% w/v)	AV (% w/v)
1	HG16	C2	20	-	-
2	HG18	C2	20	0,5	-
3	HG19	C2	20	1	-
4	HG20	C2	20	2	-
5	HG21	C2	20	-	0,5
6	HG22	C2	20	-	1
7	HG23	C2	20	-	2

3.6 Addition of Carvacrol

Varying amounts of AV and HA were incorporated into hydrogels prepared using crosslinked Ch-PEG5k conjugate with a crosslinker ratio of 20% by volume. The chemical, mechanical and morphological differences between the two materials at three different ratios were investigated. As a result of the analysis, it was determined that hydrogels containing 1% HA had the best characterization properties among the samples containing HA, while hydrogels containing 2% AV showed similar properties to 1% HA among the samples containing AV.

20 µL of carvacrol solution of 10 % by volume was added to the HG19 and HG23 hydrogel formulations. In addition, 1 µL of Tween80 and 30 µL of ethanol were used to increase the solubility of carvacrol in hydrogels.

Hydrogels with two different formulations were washed 3 times using ddH_2O and freeze-dried using lyophilization method. The chemical and morphological properties of the hydrogels in dry form were analysed.

3.7 Drug Release Studies

3.7.1 Method Development for Carvacrol

Carvacrol amounts encapsulated in hydrogel scaffolds were determined by using LC-MS/MS instrument (Agilent Technologies 6420 TripleQuad). A C18 column was used as the stationary phase and a mixture of 50 % H_2O and 50 % ACN were passed through the system with a flow rate of 0.5 mL/min. A specific MRM (Multiple Reaction Monitoring) method was developed by using the main molecular ion of carvarol molecules (Mwt: 150.22 $gmol^{-1}$). With a positive scanning mode, m/z (mass to charge) ratio for carvacrol was detected to appear with +1 charge of 150.1 Da. Different concentrations of carvacrol solutions (from 50 to 0 ppm) were prepared in acetonitrile by serial dilution and run with this MRM method, specifically prepared for carvacrol to obtain its calibration curve.

3.7.2 Drug Release Studies

The hydrogels with distinct formulations in their dry state were subjected to a release study to assess the release kinetics of carvacrol encapsulated within them. In this study, the dry hydrogels were initially encapsulated within dialysis membranes. Subsequently, the membranes were immersed in two separate solutions: 40 mL of 1X 10 mM phosphate buffer saline (PBS) with a pH of 7.4 and 40 mL of acetate buffer with a pH of 5.5. Over a period of two weeks, samples were collected at various time points (0, 0,5 1, 2 hours …..) and analysed using LC-MS/MS instrument. This analytical approach aimed to quantify the amount of carvacrol released from the hydrogels into biological environments.

4 RESULTS

4.1 Synthesis and Characterization of PEGylated Chitosan Conjugates

To obtain hydrogel structures, carboxylic acid functional groups were added to polyethylene glycol (PEG) chains with molecular weights of 2 and 5 k Da, respectively. The resulting chemical modification yield was 93% for 2kDa PEG and 91% for 5kDa PEG. In the next step, PEGs with carboxylic acid groups at one ends (PEG-COOH) were lyophilized to obtain the dried structures.

Chitosan (high molecular weight) was modified with PEG structures of different molecular weights using conjugation methods to obtain chemical groups for efficient water-solubility. In conjugation reactions, PEG5k reacted with chitosan at 82% yield, while PEG2k gave only 66% yield under similar conditions. This was followed by a detailed analysis of the conjugates using FT-IR and NMR spectroscopies.

4.1.1 Chemical Characterization of PEGylated Chitosan Conjugates

4.1.1.1 FT-IR Spectroscopy

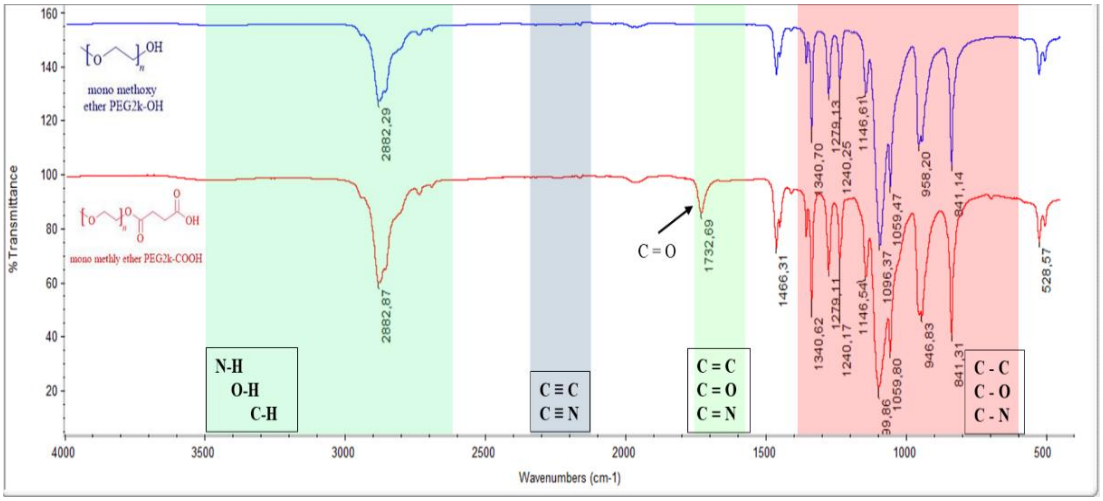

Figure 4.1 FT-IR spectra of mPEG2k-OH and mPEG2k-COOH polymers

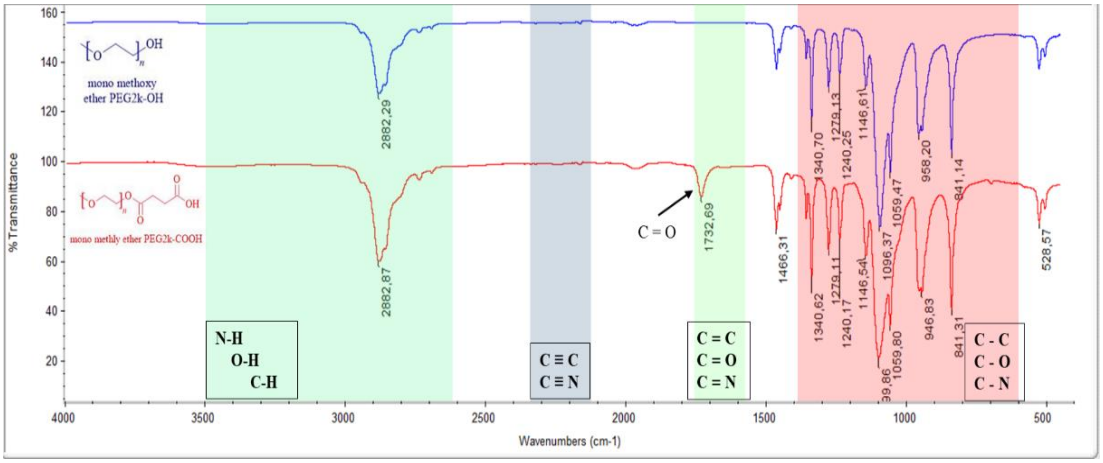

Figure 4.2 FT-IR spectra of mPEG5k-OH and mPEG5k-COOH polymers

Figures 4.1 and 4.2 present the FT-IR spectra of the chemical structures of mPEG chains with molecular weights of 2k and 5k into their respective carboxylic acid forms. Both spectra exhibit strong peaks in the 1060-1145 cm^{-1} range, representing the C-O stretching bands from the PEG backbone, and in the 2870-2960 cm^{-1} range, corresponding to C-H stretching bands. These peaks confirm that the PEG backbone structure is preserved in both samples.

The PEG-carboxylic acid groups show a distinct peak in the 1700-1750 cm^{-1} range, which corresponds to the C=O stretching vibration. In contrast, the mPEG structures do not exhibit peaks in this region. The FT-IR analysis results indicate that carboxylic acid groups have been successfully introduced into the polymer end.

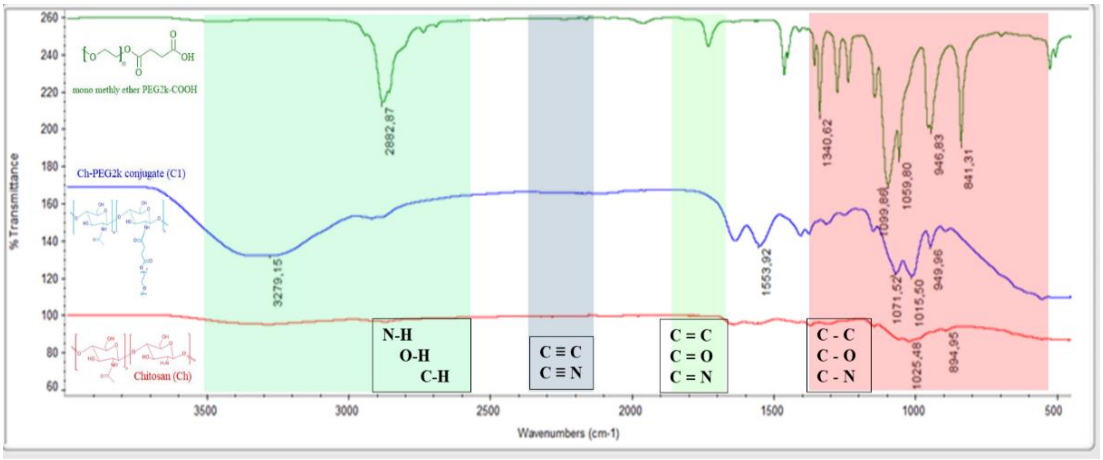

Figure 4.3 FT-IR spectra of Ch-PEG2k conjugate (C1)

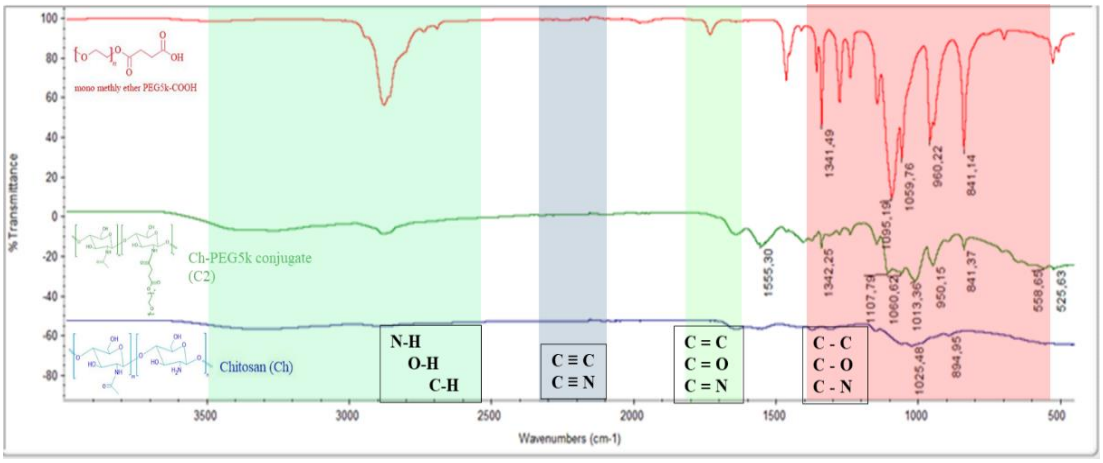

Figure 4.4 FT-IR spectra of Ch-PEG5k conjugate (C2)

Figures 4.3 and 4.4 display the obtained FT-IR spectra of conjugates synthesized using high molecular weight chitosan with PEG-COOH of 2k and 5kDa. Both conjugates have prominent peaks in the C-O stretching band in the range 1060-1145 cm^{-1} indicating the presence of PEG. In addition, peaks in the range of 1700-1750 $cm^{-1,}$ the C=O stretching band, are present in both conjugates. This peak indicates the formation of amide bonds during the conjugation process. The 3200-3500 cm^{-1} range corresponds to N-H and O-H stretching vibrations from the amino and hydroxyl groups of chitosan. Broad peaks in this region are observed in both conjugates and pure chitosan spectra. As a result of the analyses, Ch-PEG2k and Ch-PEG5k conjugates show both PEG and chitosan peaks in their chemical structures.

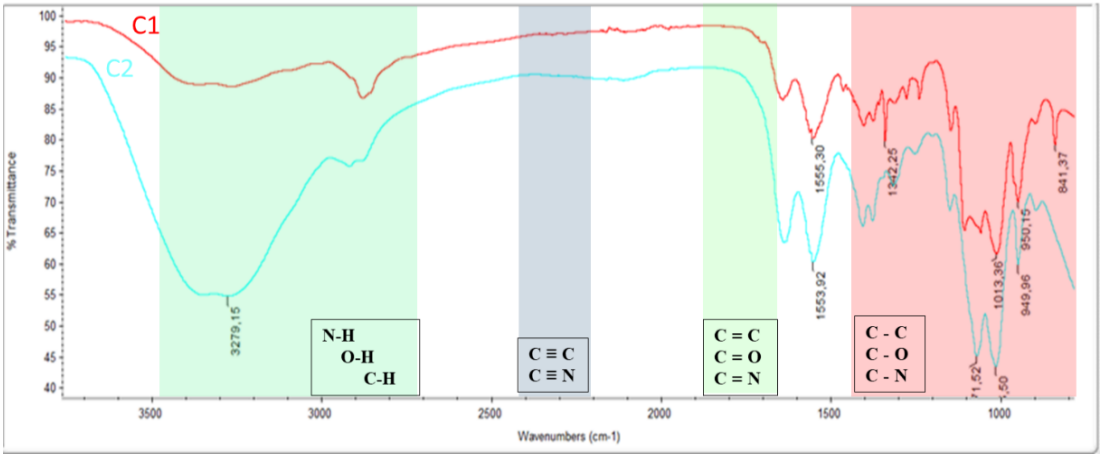

Figure 4.5 FT-IR spectra of Ch-PEG2k (C1) and Ch-PEG5k (C2)

FT-IR analyses of chitosan-PEG2k and chitosan-PEG5k conjugates confirm the presence of characteristic bonds representing the presence of both PEG and chitosan. Analysis of the spectra for both conjugates reveals distinct peaks that can be attributed to PEG and chitosan structures. Peaks in the C-O stretching band at ~1013-1100 cm^{-1} are typically assigned to C-O-C ether bonds present in PEG due to its polyether structure. These peaks are strong in both samples and indicate that the PEG component is well integrated into the conjugate structure. The peak in the C=O stretching at 1653.92 cm^{-1} in both samples corresponds to carbonyl (C=O) stretching, probably arising from the amide I band, which is characteristic of PEG-chitosan conjugates. C1 shows an overall weaker intensity, indicating a lower degree of conjugation or less presence of PEG or chitosan compared to C2.

4.1.1.2 NMR Spectroscopy

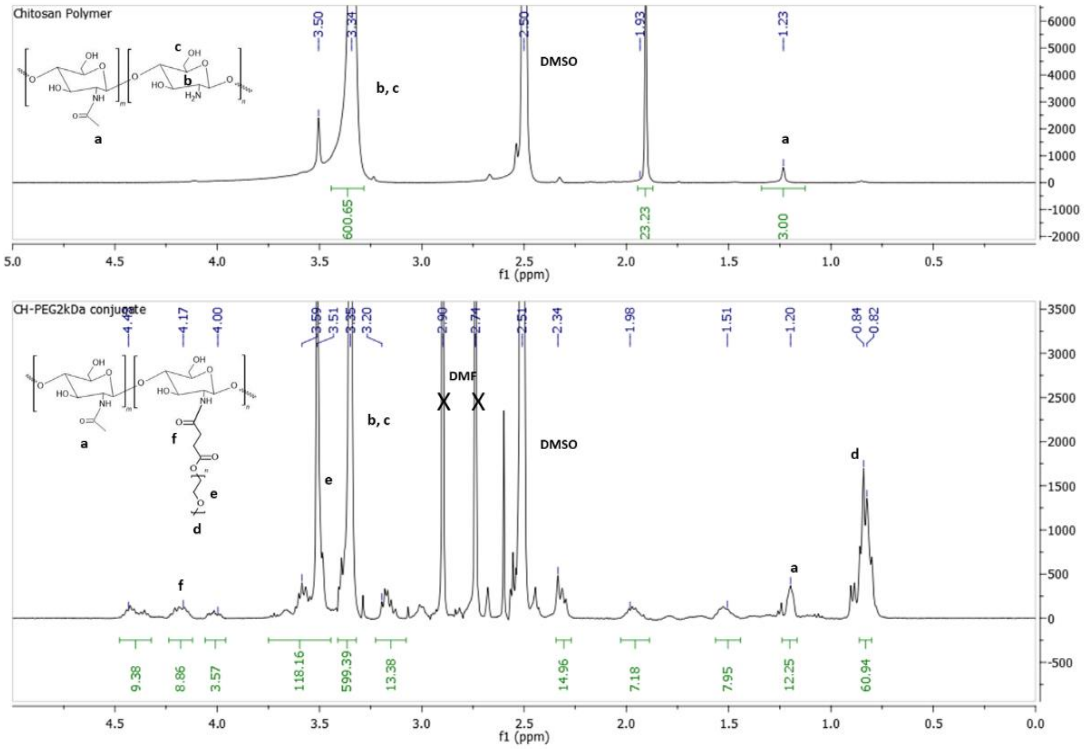

Figure 4.6 Proton NMR spectra of chitosan and Ch-PEG2k conjugate (C1)

The NMR spectra of both the native chitosan polymer and its conjugate with PEG2k (C1) were recorded to confirm the successful conjugation of PEG to chitosan.

The spectrum for the chitosan polymer exhibits characteristic signals at δ 3.50 and 3.35 ppm, which correspond to the methylene (-CH_2-) protons of the polymer backbone. The signal at δ 1.93 ppm is assigned to the N-acetyl group (-$NHCOCH_3$), which indicates partial acetylation of the chitosan. In comparison, the spectrum of the CH-PEG2k conjugate shows additional signals, particularly the peaks at δ 3.51–3.55 ppm, corresponding to the PEG methylene protons (-CH_2-CH_2-O-) integrated within the polymer backbone, confirming successful PEG conjugation. The new signals between δ 3.20–4.17 ppm further support the introduction of the PEG chain. Furthermore, the appearance of peaks around δ 0.82–1.23 ppm in the conjugate spectrum may correspond to the terminal methyl (-CH_3) groups from PEG or other aliphatic groups introduced during the conjugation process.

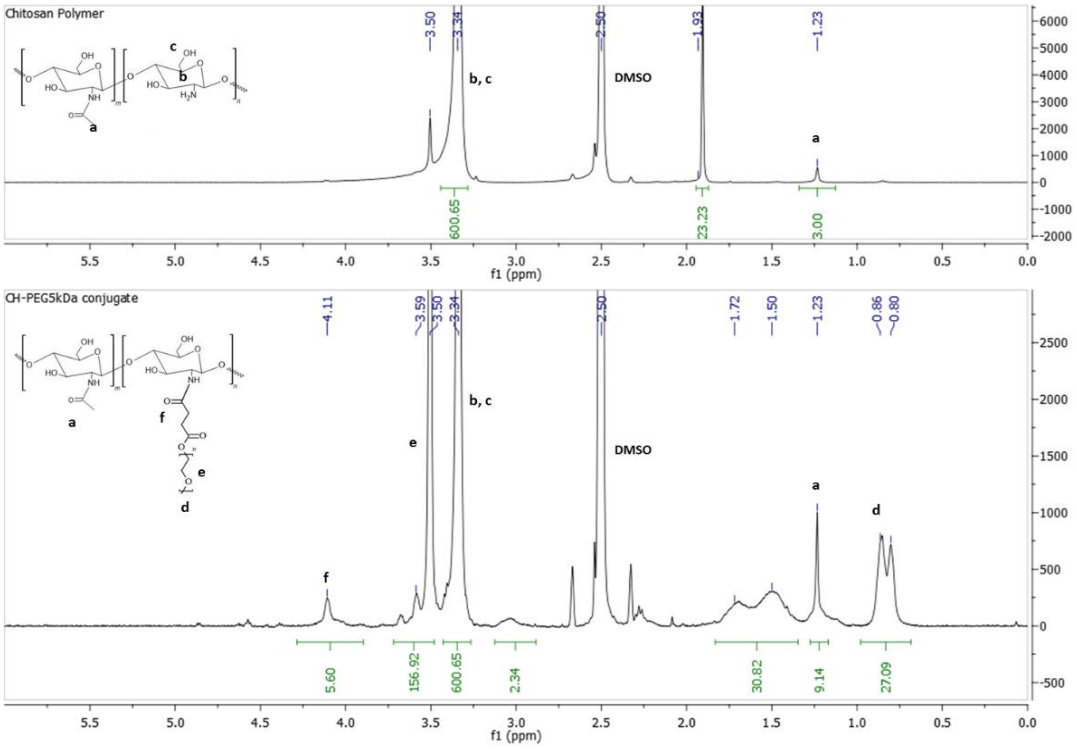

Figure 4.7 Proton NMR spectra of chitosan and Ch-PEG5k conjugate (C2)

NMR analysis of the CH-PEG5k conjugate shows that PEG5k is successfully bound to the chitosan backbone. The appearance of characteristic peaks between 3.50 ppm and 3.59 ppm corresponds to the methylene protons of the PEG chains and confirms the presence of PEG. In addition, the sharp peak at 3.20 ppm, attributed to the

ether bonds of PEG, further supports the conjugation process. These new peaks distinguish the CH-PEG5k conjugate from the native chitosan spectrum, indicating significant chemical modifications. The broader peaks between 2.90 ppm and 1.23 ppm are associated with residual signals from the chitosan backbone, indicating that the integrity of the chitosan structure is largely preserved as conjugation takes place. Furthermore, the absence of significant additional peaks in the 4.00-5.00 ppm region indicates minimal interference from by-products or unreacted components.

4.1.1.3 GPC

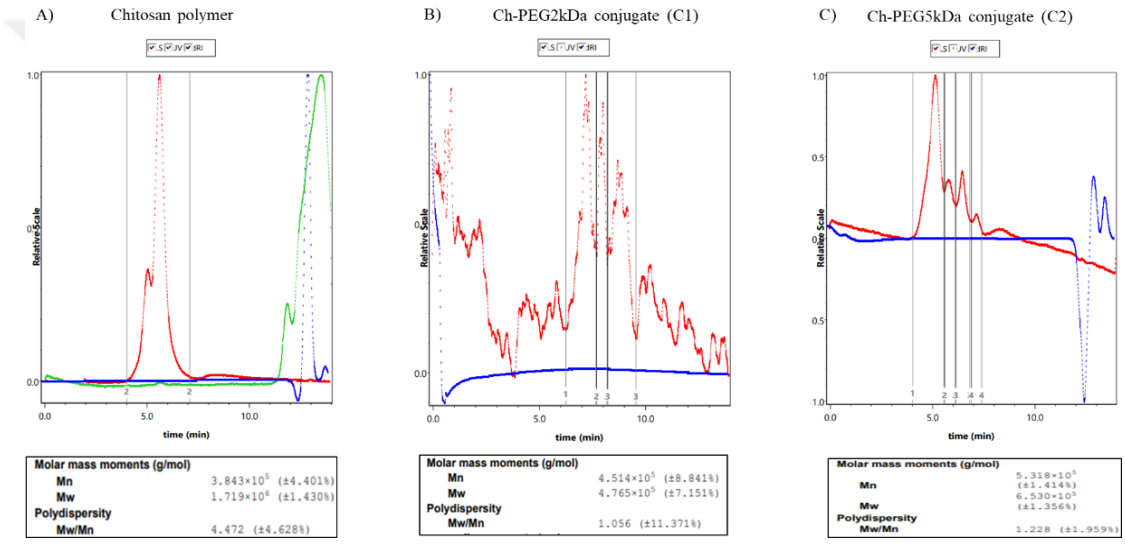

Figure 4.8 Molecular Weight Analysis of Chitosan and Conjugates by GPC (A- high molecular weight chitosan polymers, B- Ch-PEG2k conjugate (C1), C- Ch-PEG2k conjugate (C2))

The binding ratio of PEG polymer to chitosan polymer in conjugates formed with different PEG weights and named as C1 and C2 was calculated by GPC analysis and equation 1. As a result of this analysis, the binding number of C1 conjugate was calculated as 33.5 ((4.514x105 - 3.843x105) / 2000 as a result of the equation) and the binding number of C2 conjugate was calculated as 29.5 ((5.318x105 - 3.843x105) / 5000 as a result of the equation).

4.2 Hydrogel Preparation and Characterization

In order to prepare hydrogels, optimization studies were conducted by adding the crosslinker in varying ratios by weight and volume in acidic, neutral, and basic environments. These studies revealed that the neutral environment yielded better results when volume-based crosslinker additions were applied, resulting in enhanced structural stability and more efficient hydrogel formation compared to other conditions.

By crosslinking chitosan with Ch-PEG2k or Ch-PEG5k conjugates, a total of twelve distinct hydrogel samples were synthesized. Three of these were obtained by crosslinking chitosan at 65 °C with varying crosslinker ratios, and another three were prepared by crosslinking chitosan at 80°C under different crosslinker ratios. The remaining six samples were synthesized by crosslinking C1 and C2, which were produced at two different molecular weights, at 65 °C. Comprehensive chemical, physical, and morphological analyses were performed on these hydrogels to evaluate their properties.

4.2.1 Optimization of Gelation Temperature for Hydrogel Preparation

4.2.1.1 Chemical Characterization

Hydrogels were synthesized using chitosan and PEGDGE crosslinker at different activation temperatures. The chemical analysis of the hydrogels, conducted through FT-IR spectroscopy, revealed similar structural characteristics at different temperature values. In both cases, the characteristic peaks of the PEG backbone and amide bonds were observed, indicating successful crosslinking. Despite the variation in activation temperatures, the FT-IR analysis showed consistent bond formations, suggesting that the crosslinking efficiency was maintained for these samples.

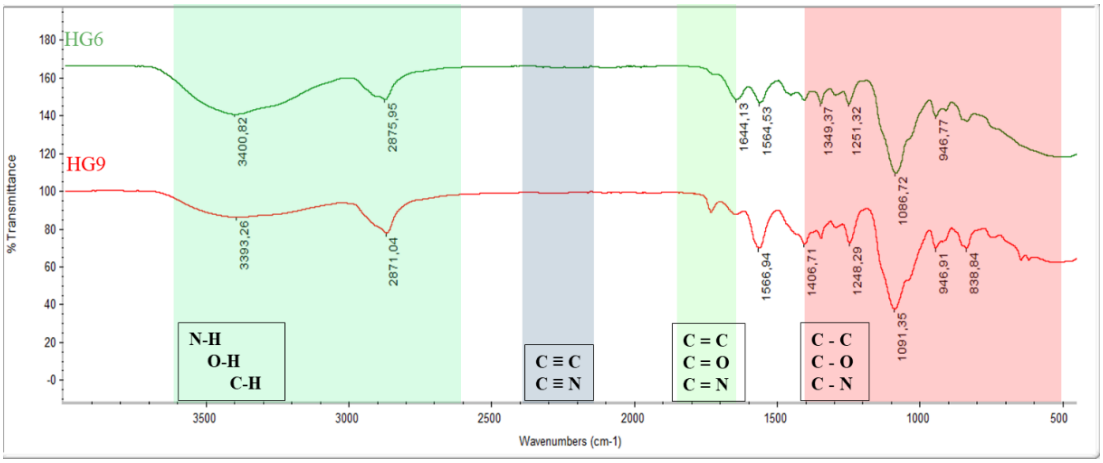

Figure 4.9 FT-IR spectra for Ch-PEGDGE10 hydrogel synthesized at crosslinker activation temperatures of 65°C (HG9) and 80 °C (HG6)

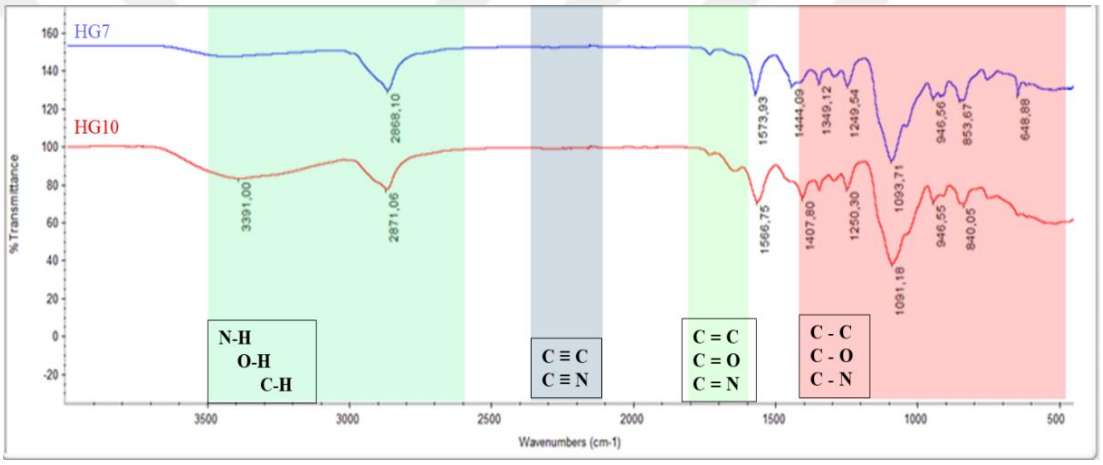

Figure 4.10 FT-IR spectra for Ch-PEGDGE20 hydrogel synthesized at crosslinker activation temperatures of 65 °C (HG10) and 80 °C (HG7)

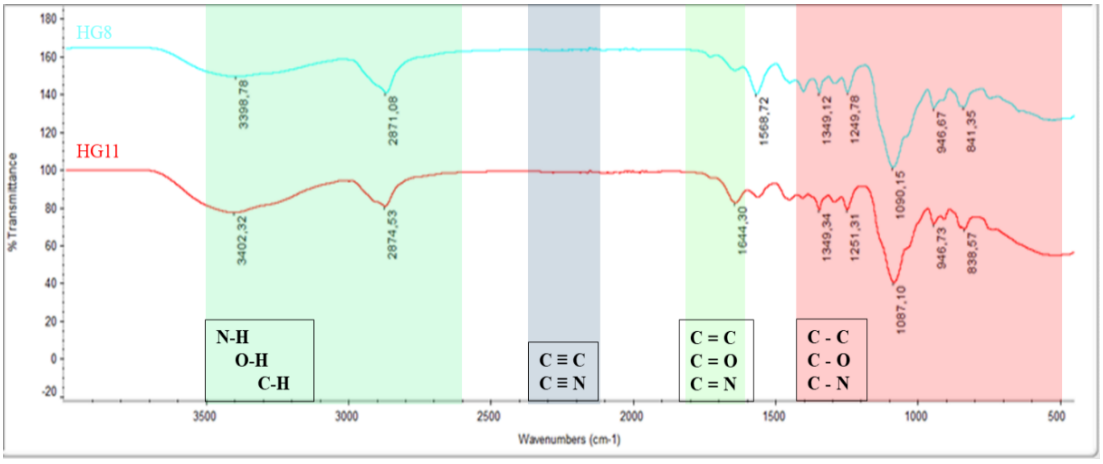

Figure 4.11 FT-IR spectra for Ch-PEGDGE40 hydrogel synthesized at crosslinker activation temperatures of 65 °C (HG11) and 80 °C (HG8)

4.2.1.2 Mechanical Characterization

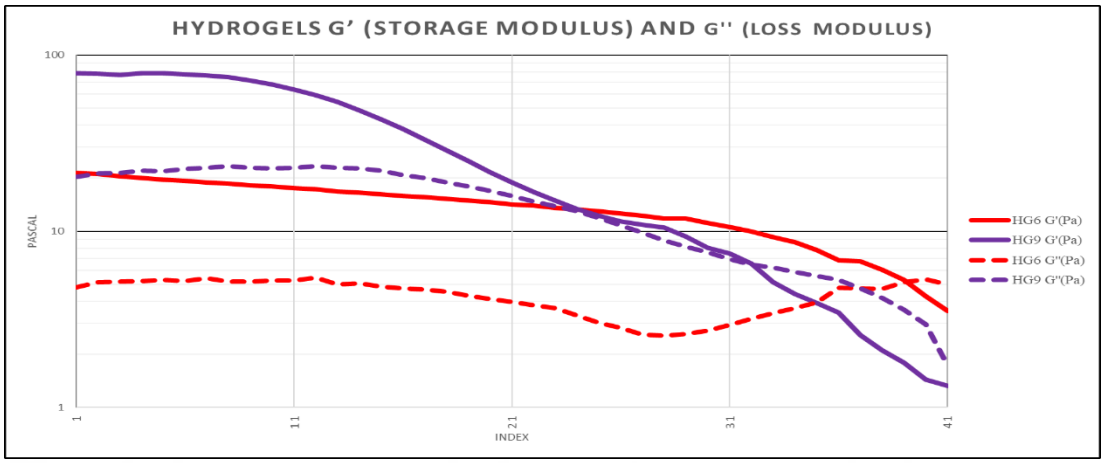

Figure 4.12 Comparison of elastic modulus (G' and G’’) for different Ch-PEGDGE10 Hydrogels at 65 °C G'(Pa) and 80 °C G'(Pa)

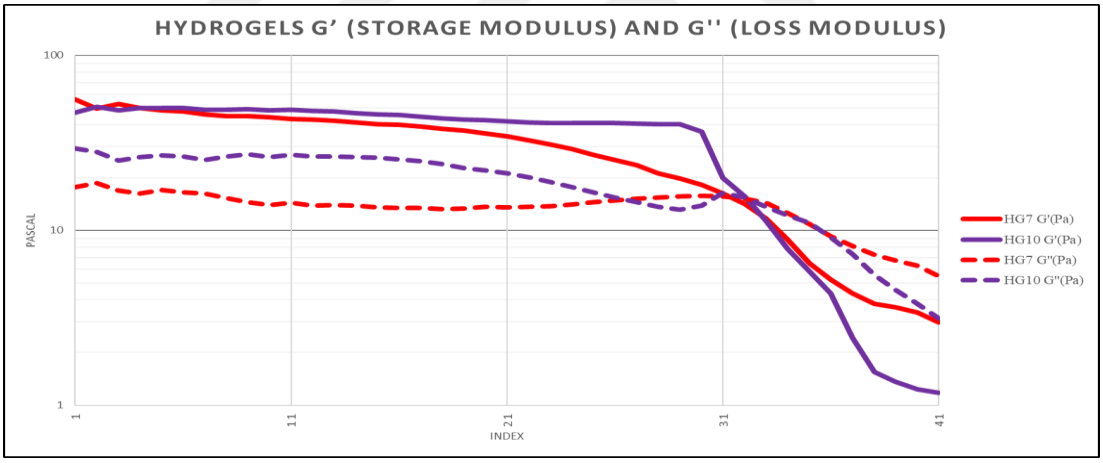

Figure 4.13 Comparison of elastic modulus (G' and G’’) for different Ch-PEGDGE20 Hydrogels at 65 °C G'(Pa) and 80 °C G'(Pa)

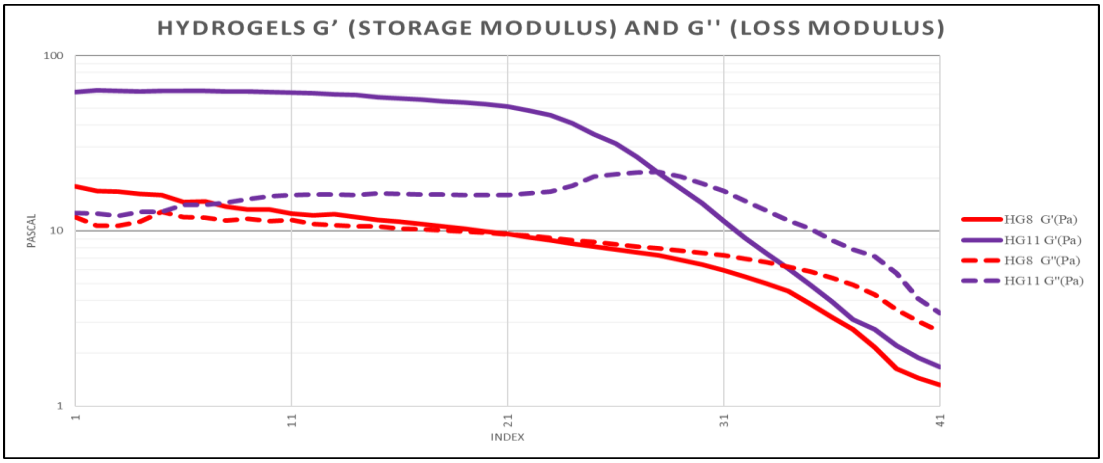

Figure 4.14 Comparison of elastic modulus (G' and G’’) for different Ch-PEGDGE40 Hydrogels at 65 °C G'(Pa) and 80 °C G'(Pa)

Hydrogels formed at 65 and 80 ºC by adding 10, 20 and 40% by volume of crosslinker to chitosan were compared in terms of their mechanical properties. Three groups formed by grouping hydrogels with the same amount of crosslinker were compared within themselves. As a result of this comparison, it was measured that the hydrogels formed at 65 °C had higher G' and G" values compared to the hydrogels formed at 80 °C. With the effect of increasing pressure, all hydrogels entered the degradation process.

4.2.2 Characterization of Stable Hydrogels

4.2.2.1 Conversion of Hydrogels

Table 4.1 Conversion of Hydrogels prepared at 65 ºC

Material	Crosslinker ration (%)		
	10%	**20%**	**40%**
Chitosan	35,29	28,96	28,1
C1	31,93	21,67	34,7
C2	18,8	74,24	51,3

Table 4.1 shows gel conversion ratios of hydrogels synthesised at 65 °C using chitosan, Ch-PEG2k (C1) and Ch-PEG5k (C2) conjugates. According to the results, it was found that the hydrogels produced with Ch-PEG5k conjugate were obtained with higher efficiency and showed better mechanical properties. Also, the hydrogels containing Ch-PEG5k conjugate formed more stable structures and reached higher conversion regardless of the crosslinker density.

4.2.2.2 Chemical Characterization

The FT-IR analysis results show that chemical bonds were successfully formed in hydrogels synthesized with different weight Ch-PEG conjugates and chitosan. The FTIR spectra confirm that the desired chemical structures were obtained in each case with characteristic absorption bands corresponding to the expected bond formations. The prominent peaks between 1000-1100 cm^{-1} are due to C-O stretching vibrations confirming the presence of ether bonds from the PEG backbone in the hydrogels. The fingerprint region of the spectra, especially between 800-600 cm^{-1}, shows several peaks corresponding to various bending vibrations in the polymer chains, further supporting the successful formation of hydrogels.

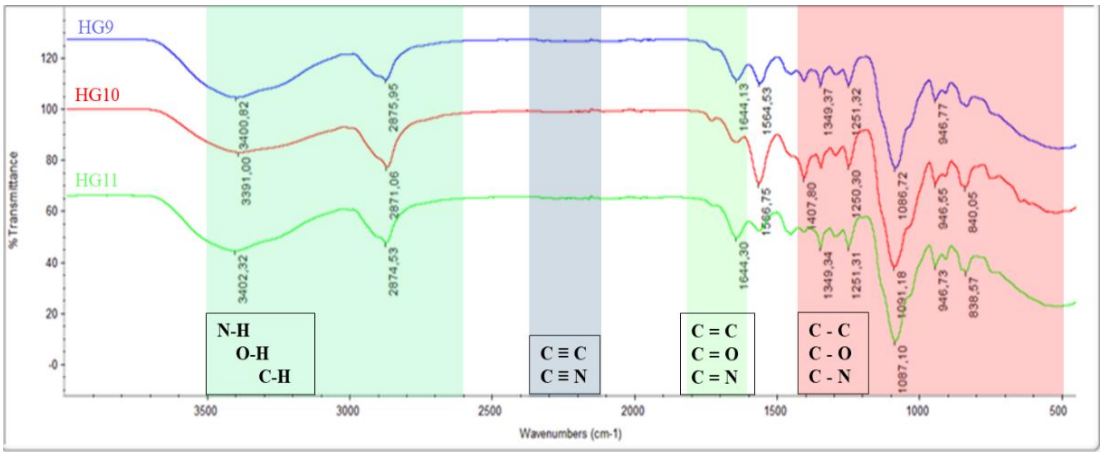

Figure 4.15 FT-IR spectra of the Ch-PEGDGE10 (HG9), Ch-PEGDGE20 (HG10) and Ch-PEGDGE10 (HG11)

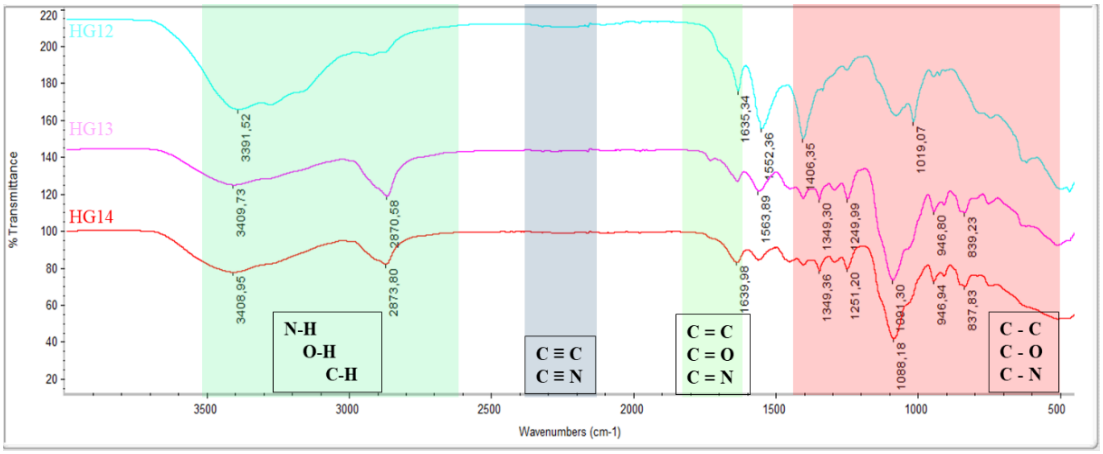

Figure 4.16 FT-IR spectra of Ch-PEG2k-PEGDGE10 (HG12), Ch-PEG2k-PEGDGE20 (HG13) and Ch-PEG2k-PEGDGE40 (HG14)

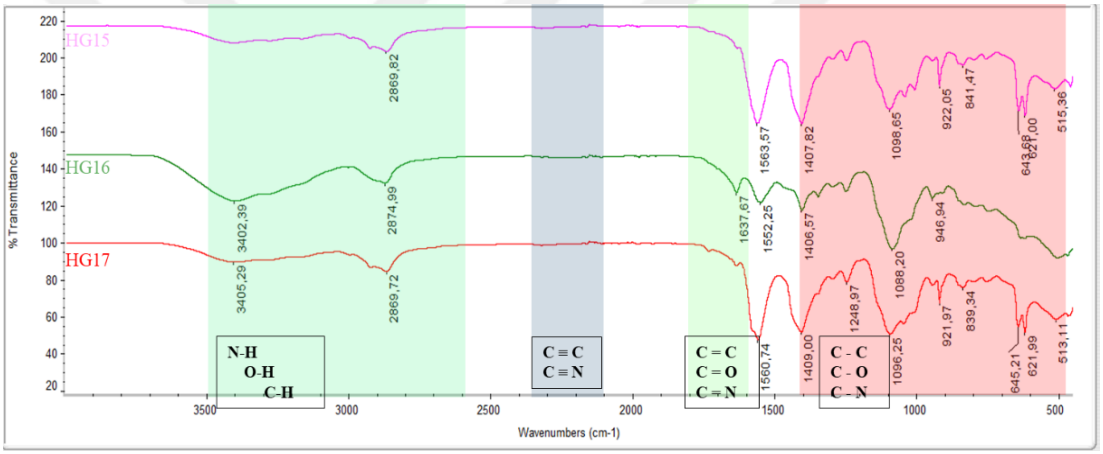

Figure 4.17 FT-IR spectra of Ch-PEG5k-PEGDGE10 (HG15), Ch-PEG5k-PEGDGE20 (HG16) and Ch-PEG5k-PEGDGE40 (HG17)

4.2.2.3 Mechanical Characterization

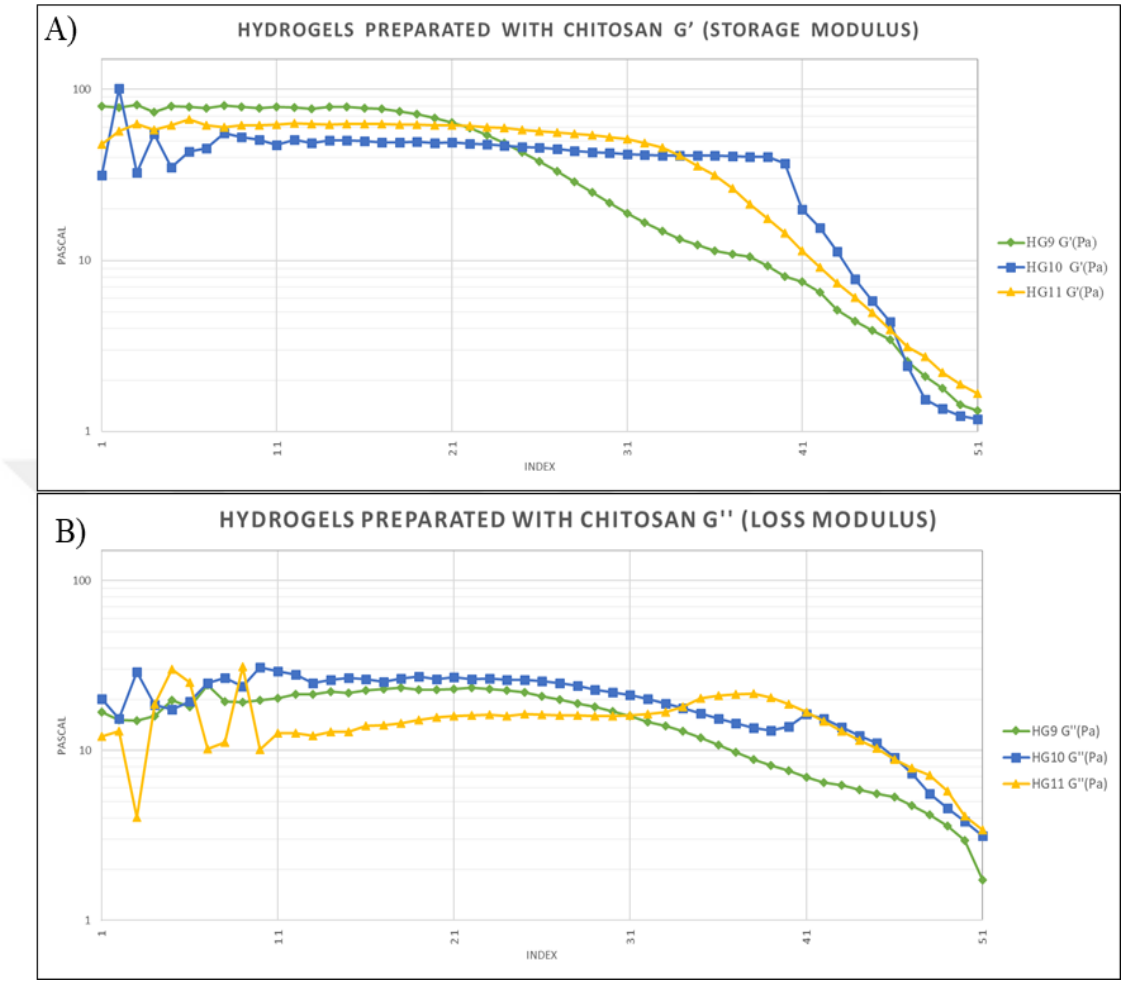

Figure 4.18 Comparison of elastic modulus (G') and viscous modulus (G") values of hydrogels of chitosan with different crosslinker percentages (A- Comparison of G' value, B- Comparison G'' Value)

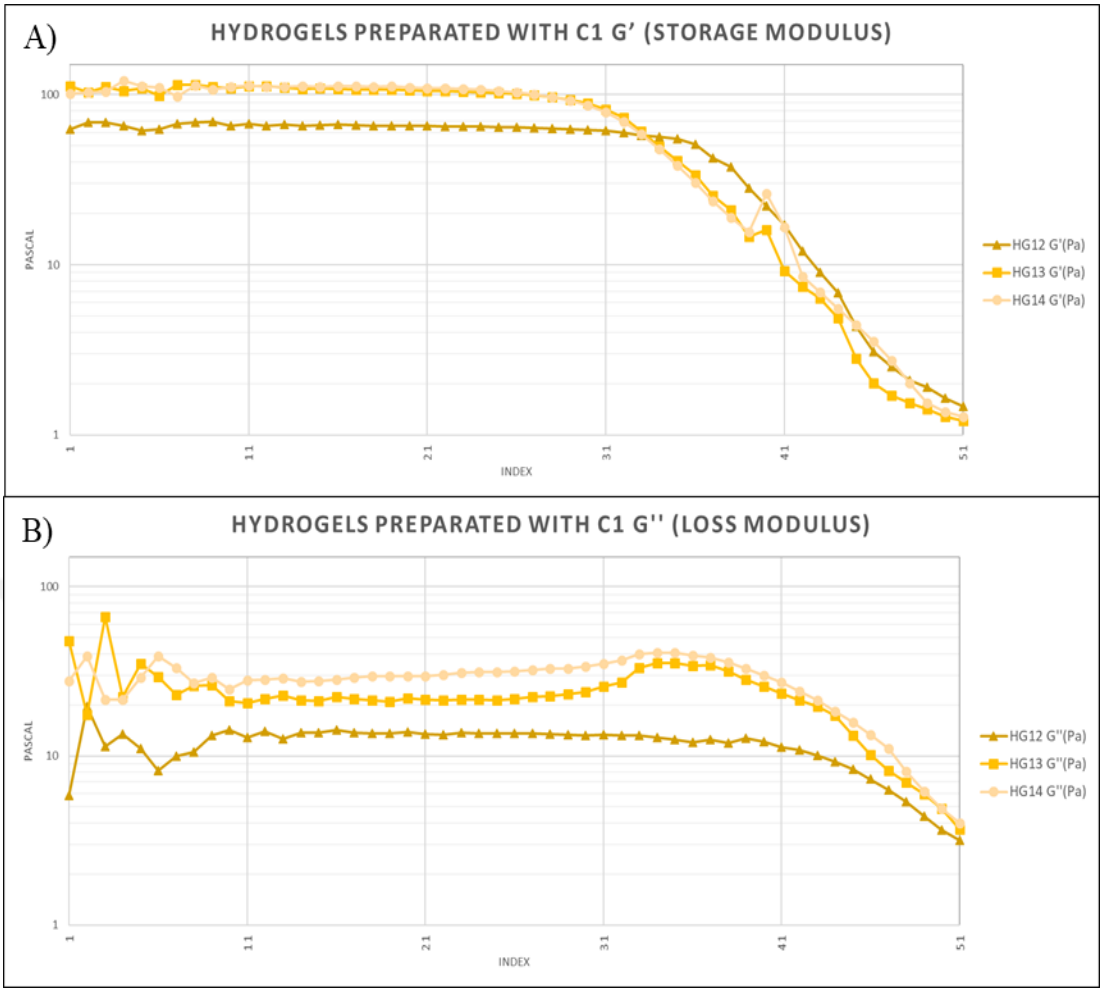

Figure 4.19 Comparison of elastic modulus (G') and viscous modulus (G") values of hydrogels of Ch-PEG2k conjugate (C1) with different crosslinker percentages (A- Comparison of G' value, B- Comparison of viscous modulus G" values)

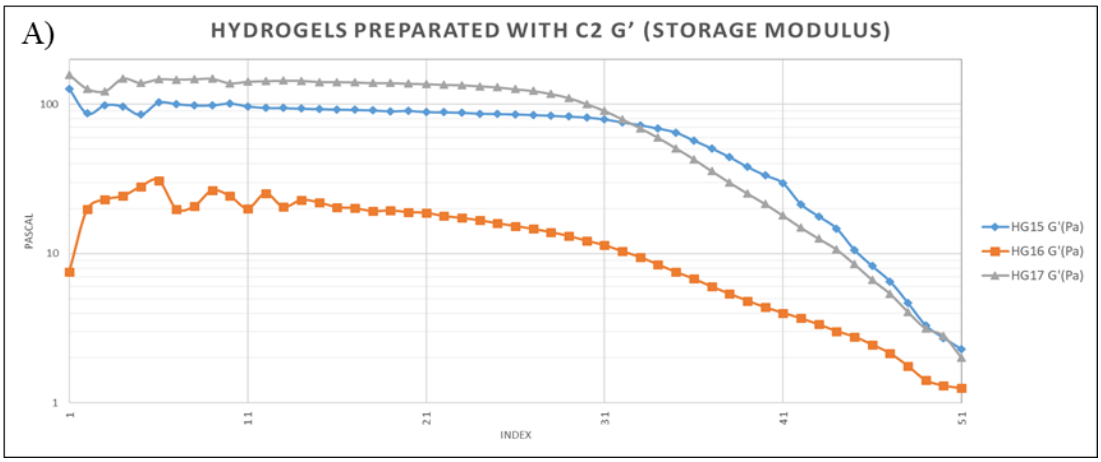

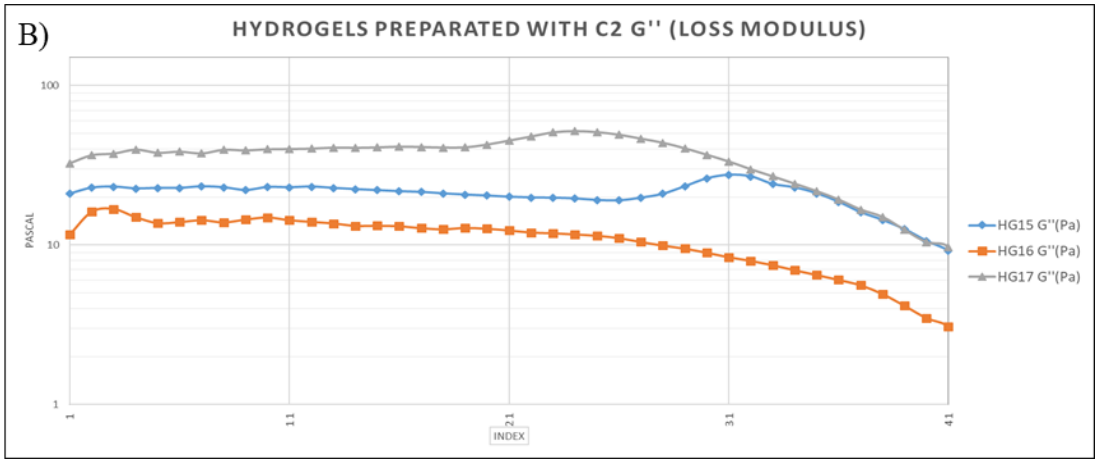

Figure 4.20 Comparison of elastic modulus (G') and viscous modulus (G") values of hydrogels of Ch-PEG5k conjugate (C2) with different crosslinker percentages (A-Comparison of G' value, B- Comparison of viscous modulus G" values)

The gels formed by adding different ratios of crosslinker to Chitosan, Ch-PEG2k and Ch-PEG5k conjugates were subjected to mechanic characterization using a rheometer. As a result of these characterization steps, it was understood that gelation occurred in all assemblies. With the effect of the applied force over time, the hydrogel structures entered into a degradation process and lost their mechanical properties.

4.2.2.4 Swelling Studies

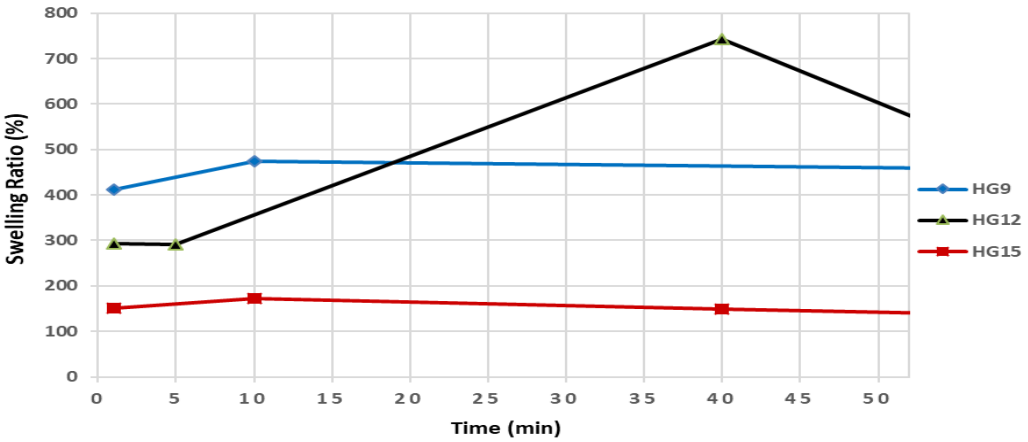

Figure 4.21 Swelling profiles for hydrogels crosslinked with 10% PEGDE. (HG9: chitosan, HG12: Ch-PEG2k, HG15: Ch-PEG5k)

Percentage swelling values for hydrogels formed with chitosan, Ch-PEG2k, Ch-PEG5k conjugates over time was calculated. When the remaining samples were compared, it was understood that the initial percentages and swelling capacities of the samples obtained by adding crosslinker at different ratios to Chitosan and Ch-PEG2k conjugate were higher. The samples formed with Ch-PEG5k, where the PEG concentration is higher, have less water retention and have a more stable swelling rate.

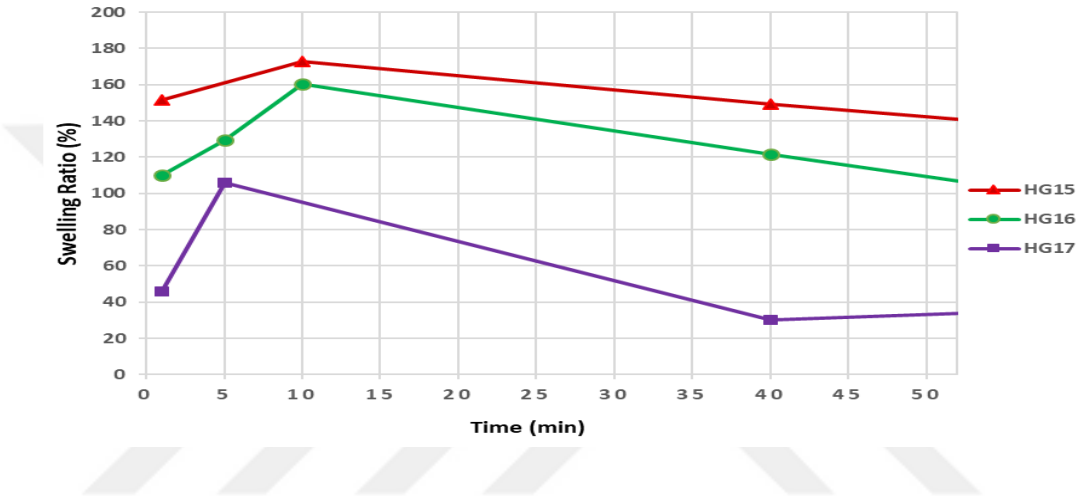

Figure 4.22 Swelling profiles for hydrogels prepared with C2 (Ch-PEG5k). (HG15: 10% PEGDE, HG16: 20% PEGDE, HG17: 40% PEGDE)

The swelling behaviour of the hydrogels formed with Ch-PEG5k conjugates over time was calculated over time as a percentage. It was observed that the hydrogel formed by adding 40% by volume of crosslinker to the Ch-PEG5k conjugate shows increases and decreases during the analysis and these variations indicate a less stable system. The water retention levels of the other hydrogels were observed to increase first and then to decrease in water retention capacity by undergoing a degradation process.

4.2.2.5 Morphological Analysis

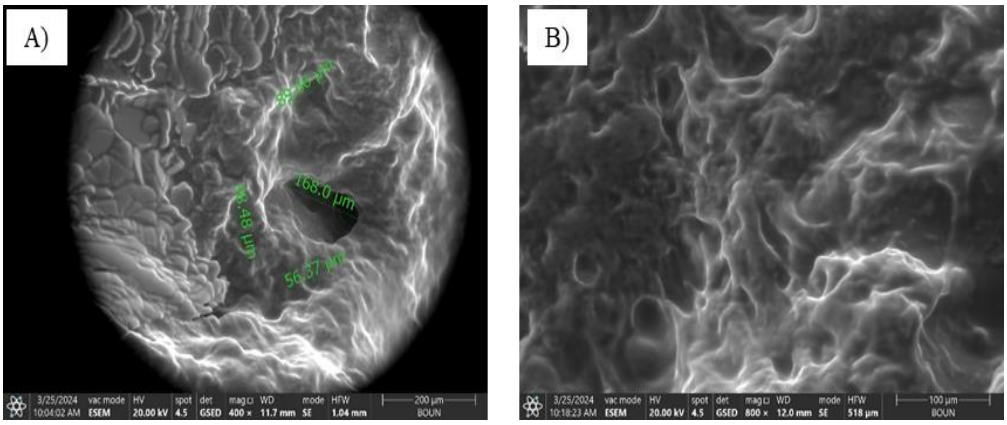

Figure 4.23 Morphological Imaging of Ch-PEG5k-PEGDGE20 (HG16) hydrogel (magnification: A-400x, B-800x)

The morphological structure of hydrogels formed by adding 20% by volume of crosslinker to Ch-PEG5k conjugates was characterization using ESEM. The results of this characterization showed that the hydrogel has a porous structure of different sizes and shapes between 50-200 μm.

4.3 Addition of Hyaluronic Acid and Aloe Vera to Hydrogels

As a result of the characterizes of 9 hydrogels formed with chitosan, Ch-PEG2k and Ch-PEG5k conjugates with 10, 20 and 40% crosslinkers by volume, the hydrogel with 20% crosslinker by volume formed with Ch-PEG5k conjugate was selected as the most optimal hydrogel. To this hydrogel, HA and AV were added at the ratios of 0,5 , 1 and 2 wt% and 6 different compositions of hydrogels were obtained.

4.3.1 Conversion of Hydrogels with HA or AV

Table 4.2 Conversion of hydrogels containing HA or AV

Hydrogels	**% of added material (w/v)**		
	0,50%	**1%**	**2%**
HG16-HA	24,57	20,37	37,24
HG16-AV	10,08	6,99	13,04

In Table 4.2, conversion ratios were calculated from the dry weights of the hydrogels formed by adding different ratios of Hyaluronic Acid and Aloe vera by weight to Ch-PEG5k-PEGDGE20 (HG16) hydrogel. At the end of the characterizations, hydrogel formed with HA was observed to have a higher conversion rate, in other words, a more bulk structure, compared to the hydrogels formed with AV. In addition, no linear relationship was found between the increase in the percentage of AV or HA and the conversion.

4.3.2 Chemical Characterization of Hydrogels with HA or AV

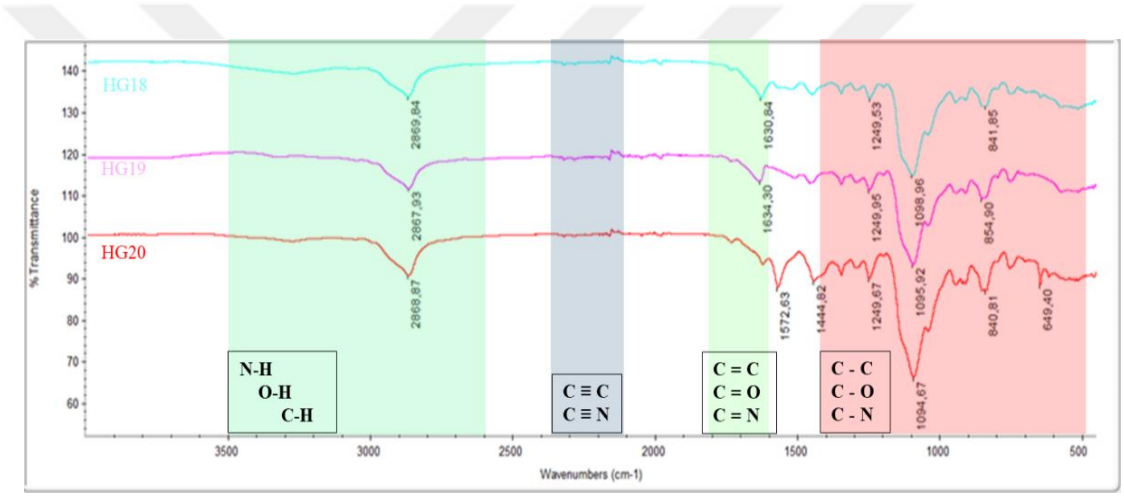

Figure 4.24 FT-IR spectra of Ch-PEG5k- PEGDGE20-HA0.5 (HG18), Ch-PEG5k-PEGDGE20-HA1 (HG19) and Ch-PEG5k-PEGDGE20-HA2 (HG20)

In Figure 4.24, the chemical properties of the hydrogels formed by adding different ratios of Hyaluronic Acid and by weight to the HG16 were analysed using FT-IR. As a result of these characterises, strong evidence of HA bond structure was found. Peaks were measured in the C=O stretching region corresponding to 1600-1650 cm^{-1}, called the Amide I band, in HG18 and HG19 hydrogels. (58) In HG20 hydrogel, peaks were observed in the C=O stretching region corresponding to 1400-1450 cm^{-1}, which is called carboxyl group.

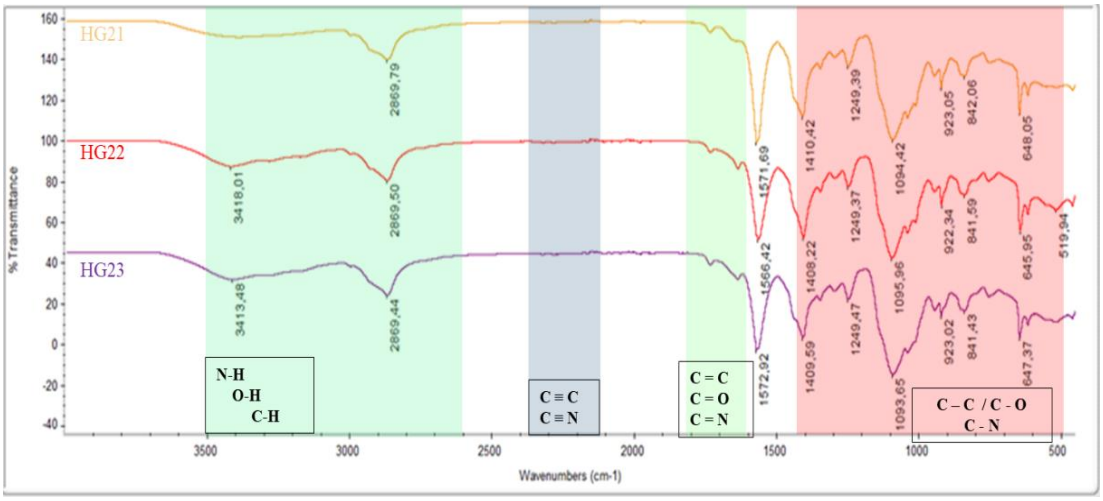

Figure 4.25 FT-IR spectra of Ch-PEG5k-PEGDGE20-AV0.5 (HG21), Ch-PEG5k-PEGDGE20-AV1 (HG22) and Ch-PEG5k-PEGDGE20-AV2 (HG23)

In Figure 4.25, the chemical properties of the hydrogels formed by adding different ratios of Aloe vera by weight to the HG16 hydrogel were analysed using FT-IR. As a result of these analyses, strong evidence of AV bond structure was found. The O-H stretching in the range of approximately 3200-3500 cm^{-1} is related to the hydroxyl groups abundant in Aloe Vera due to its polysaccharide content. (59) The presence of this bond in HG22 and HG23 has been proven.

4.3.3 Mechanical Characterization of Hydrogels with HA or AV

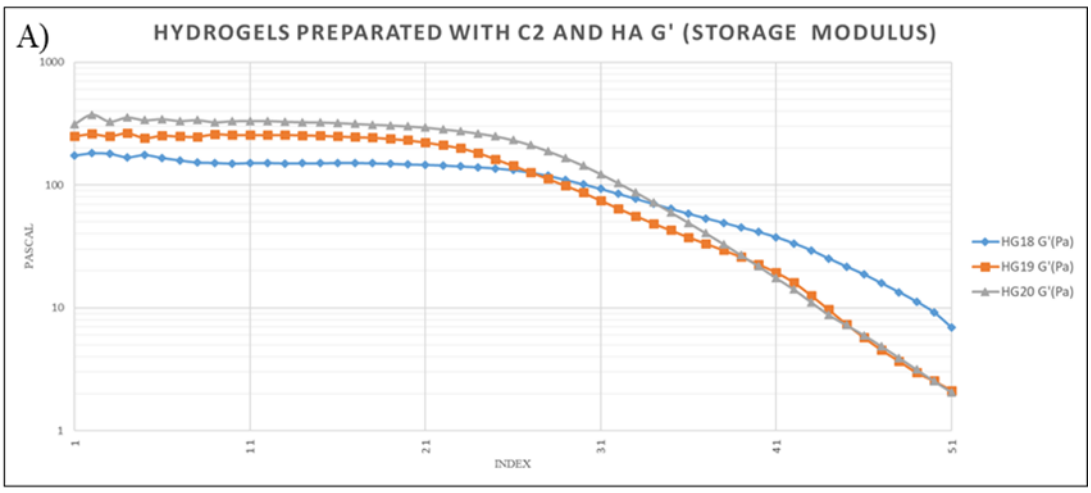

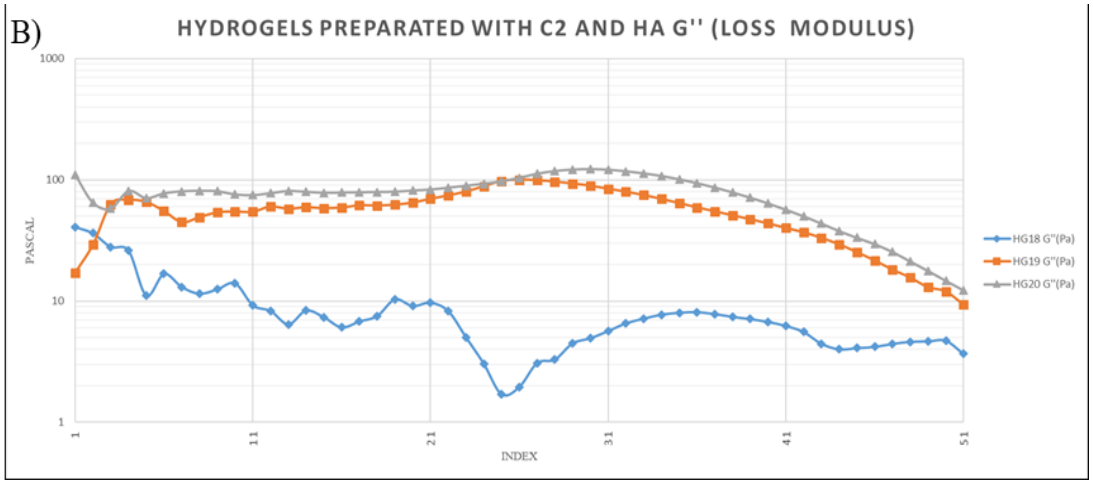

Figure 4.26 Comparison of G' and G" values of HG16 at different HA percentages (A-comparison of G' value, B- comparison G'' Value)

The mechanical properties of 3 different hydrogels formed by adding different ratios of HA by weight to HG16 were measured by rheometer. In all gels, the initial G' value is above the G" value, which proves that the hydrogels show properties solid-like. As the HA content in the hydrogels increased, the initial G' values were observed to be even higher. With the effect of increasing pressure over time, all hydrogels entered the degradation process.

While HG19 and HG20 showed more stable properties, the mechanical properties of HG18 hydrogel were not stable.

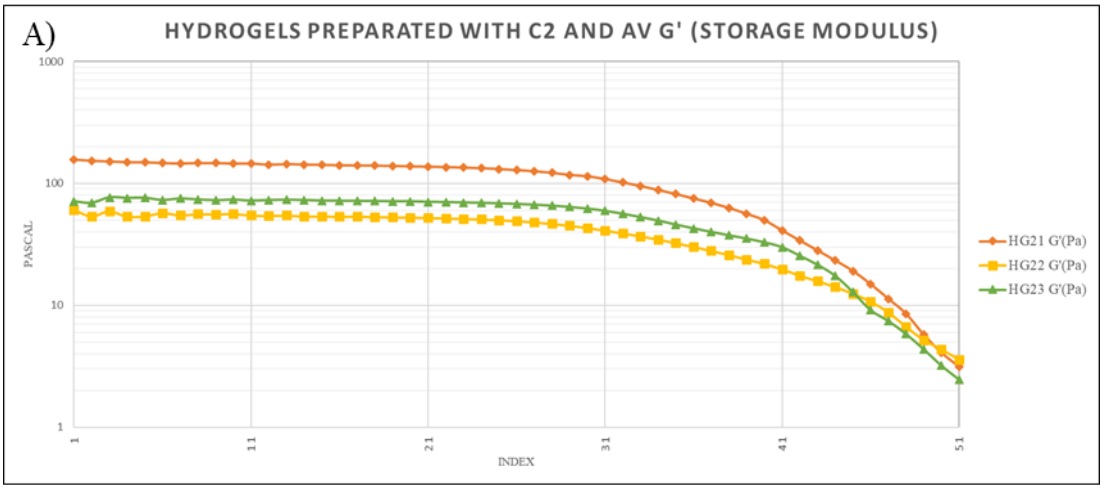

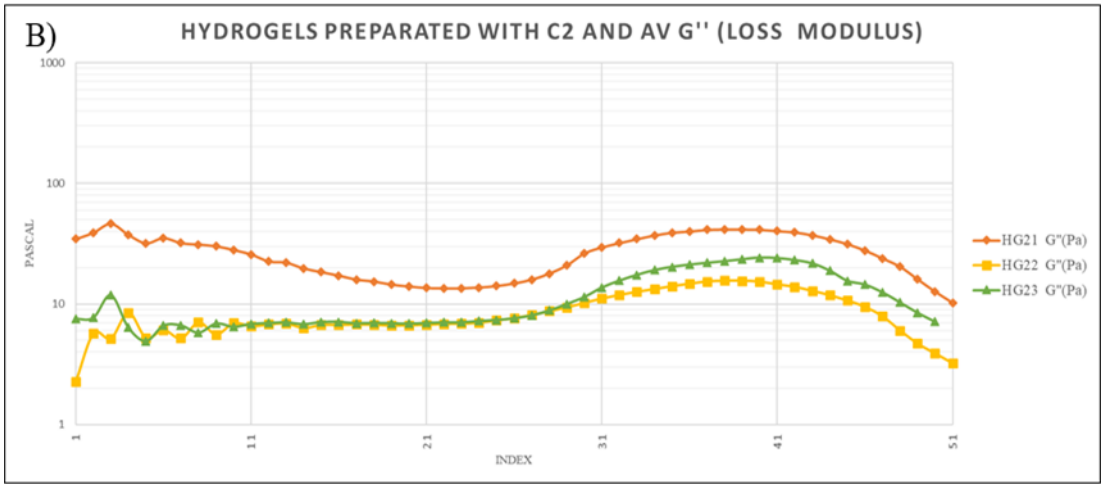

Figure 4.27 Comparison of G' and G" Values of HG16 Hydrogel at Different AV Percentages (A- Comparison of G' value, B- Comparison G'' Value)

Mechanical properties of 3 different hydrogels including AV at different ratios (by weight) were measured by rheometer. Initially, the G' value is above the G" value in all gels, which proves that the hydrogels show properties solid-like. It was observed that the initial G' values decreased further as the AV content in the hydrogels increased. With the effect of increasing pressure over time, all hydrogels entered the degradation process.

4.3.4 Swelling Studies of Hydrogels with HA or AV

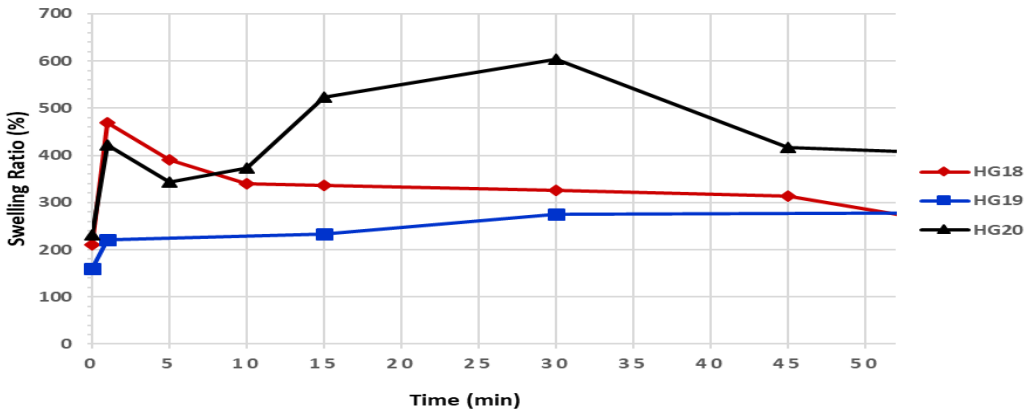

Figure 4.28 Swelling profiles for hydrogels prepared with C2 (Ch-PEG5k) and 40% PEGDE. (HG18: 0.5% HA, HG19: 1% HA, HG20: 2% HA)

The swelling behaviour of the hydrogels over time was analysed by adding different ratios of HA by weight to the HG16 structure. As a result of these analyses, HG18 hydrogel showed a swelling of approximately 500% in the first 5 minutes and then its physical structure deteriorated and entered the degradation process. HG19, on the other hand, showed less swelling and had a swelling percentage between 100-300% and maintained this stabilized state for a long time. HG20 has a swelling percentage of 200-600%, but there are increases and decreases at irregular intervals which do not show a stable profile.

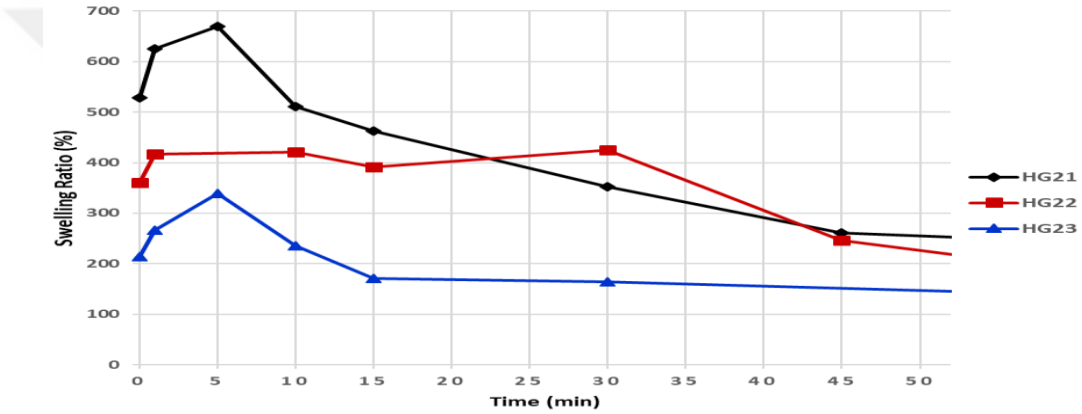

Figure 4.29 Swelling profiles for hydrogels prepared with C2 (Ch-PEG5k) and 40% PEGDE. (HG21: 0.5% AV, HG22: 1% AV, HG23: 2% AV)

The swelling behaviour of the hydrogels over time was analysed by adding different ratios of AV by weight to the HG16 structure. As a result of these analyses, HG21 and HG23 showed maximum swelling in the first 5 minutes and then their physical structure deteriorated and entered the degradation process. The swelling percentages of the two hydrogels are different; HG21 has a maximum swelling percentage of around 700% while HG23 has a maximum swelling percentage of 350%. The HG22 did not show a stable increase or decrease with time.

4.3.5 Morphological Characterization of Hydrogels with HA or AV

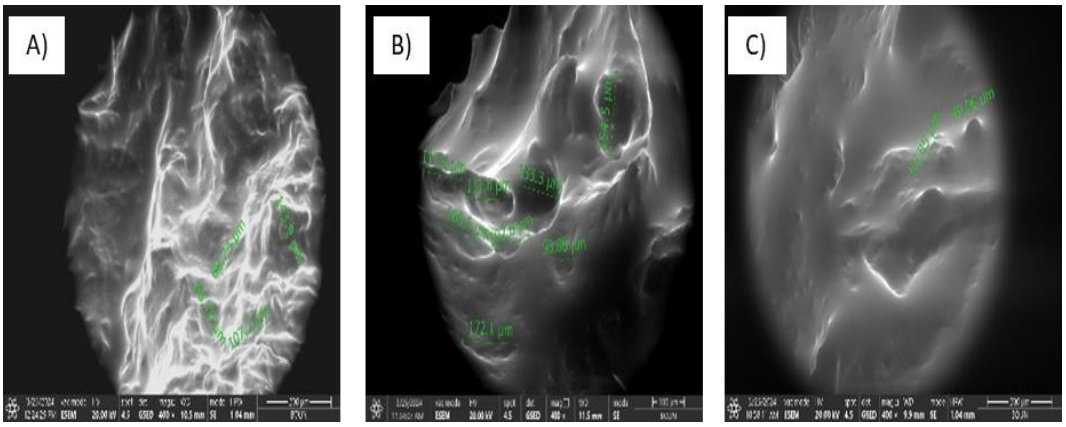

Figure 4.30 Morphological Imaging of HG16 with different HA ratio (A- HG18 (Ch-PEG5k-PEGDGE20-HA0,5) , B- HG19 (Ch-PEG5k-PEGDGE20-HA1) C- HG20 (Ch-PEG5k-PEGDGE20-HA2)

The hydrogels of HG16 were added HA polymer at the ratios 0.5, 1 and 2 wt % and then were lyophilized for morphological analysis in ESEM mode in SEM. It was found that the pore structure decreased by adding HA into HG16. The increase in the amount of HA showed a direct proportion to decrease in pore size. The pores had a measured size of 80–150 μm in HG18 with 0.5% HA. On the other hand, HG19 with 1% HA provided pores was between 50–180 μm, and the few pores identified in HG20 with 2% had a diameter near to 50 μm.

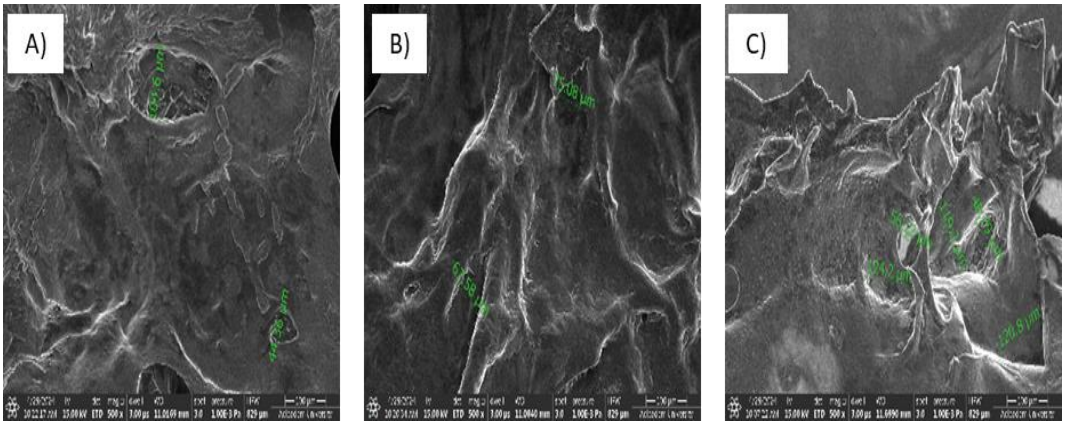

Figure 4.31 Morphological Imaging of HG16 with different AV ratio (A- HG21 (Ch-PEG5k-PEGDGE20-AV0,5), B- HG22 (Ch-PEG5k-PEGDGE20-AV1) C- HG23 (Ch-PEG5k-PEGDGE20-AV2)

Hydrogels formed by adding AV to HG16 structure at the ratios of 0.5, 1 and 2 wt% were subjected to morphological analysis by SEM device after the lyophilisation process. As a result of these analyses, it was observed that the pore structure increased as a result of AV into the HG16 hydrogel. The increase is directly proportional to the increase in the amount of HA. The pore sizes were between 30-200 μm in HG21 (with 0,5 % AV) , between 50-200 μm in HG22 (with 1,0% AV) and around 50-150 μm in HG23 (with 2,0% AV) hydrogel.

4.4 Carvacrol Loaded Hydrogel

For further research, HG19 is chosen, as it is the most promising from hydrogels formed by combinig 0.5, 1 and 2 wt % of HA to the HG16 structure. In addition, HG23 is also chosen, second from hydrogels formed by adding AV to the HG16 structure at 0.5, 1, and 2 wt%, as it is most similar to HG19. As an extension to these formulation, carvacrol molecule was included into system to demonstrate its therapeutic effect. Conversion ratios were calculated for hydrogels with various carvacrol amounts and their chemical and morphological properties were evaluated.

4.4.1 Conversion of Hydrogel with Carvacrol

Table 4.3 Conversion of HG19 and HG23 hydrogel with carvacrol

Hydrogel	Conversion (%w/v)
HG24 (Ch-PEG5k-PEGDGE20-HA1-CA)	14,26
HG25 (Ch-PEG5k-PEGDGE20-AV2-CA)	7,85

HG19 and HG23 were co-assembled with HA or AV and loaded with carvacrol. Thus, the gel conversion values of these scaffold were calculated after the freeze-drying process. When HG24 and HG25 hydrogels were compared among themselves, it was calculated that HG24 with HA content had 2 times the conversion compared to HG25.

4.4.2 Chemical Characterization of Carvacrol-loaded Hydrogels

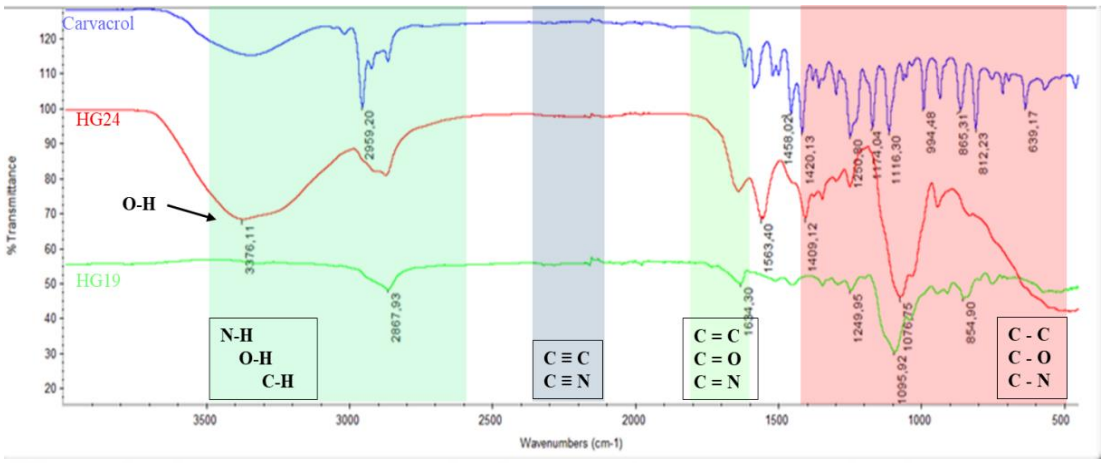

Figure 4.32 FT-IR spectra of pure carvacrol, Ch-PEG5k-PEGDGE20-HA1 (HG19), and Ch-PEG5k-PEGDGE20-HA1-CA (HG24)

The hydrogel designated HG24 represents the incorporation of carvacrol into the hydrogel matrix. In the chemical structure analysis obtained by FT-IR, the carvacrol structure was successfully incorporated into the hydrogel. The broad peak at 3376.11 cm^{-1} is an indicative of O-H stretching, similar to the pure carvacrol analysis, but slightly shifted, indicating hydrogen bonding interactions between carvacrol and the hydrogel. The peak seen at 1598.30 cm^{-1} also shows the stretching vibration of aromatic C=C and can refer to carvacrol having an aromatic ring in its chemical structure. (60)

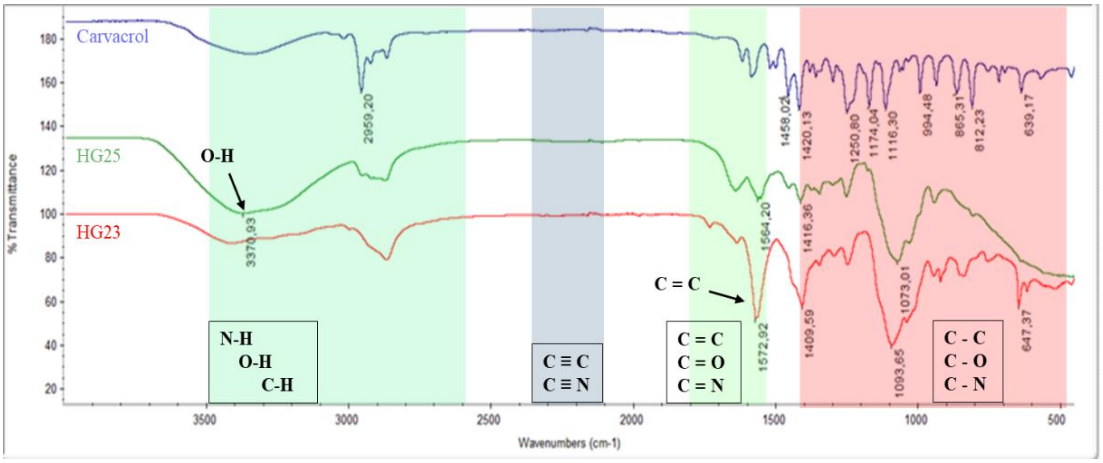

Figure 4.33 FT-IR spectra of pure carvacrol, Ch-PEG5k-PEGDGE20-AV2 (HG23), and Ch-PEG5k-PEGDGE20-AV2-CA (HG25)

The hydrogel, designated as HG25, represents the incorporation of carvacrol into the hydrogel matrix. The spectrum of FT-IR showed that the structure carvacrol molecules were effectively incorporated into the hydrogel. The wide peak at 3371.03 cm^{-1} includes the O–H stretching, as observed in pure carvacrol but slightly shifted, pointing to hydrogen bonding interactions between Carvacrol and hydrogel formulations. The peak at 1524.20 cm^{-1} also represents aromatic C=C stretching vibration and suggests Carvacrol seems to contain a phenyl ring in its structure. There were also new shifts and peaks observed in the fingerprint region (1000-1500 cm^{-1}), indicating chemical interactions between Carvacrol and the hydrogel components.

4.4.3 Morphological Characterization of Hydrogels with Carvacrol

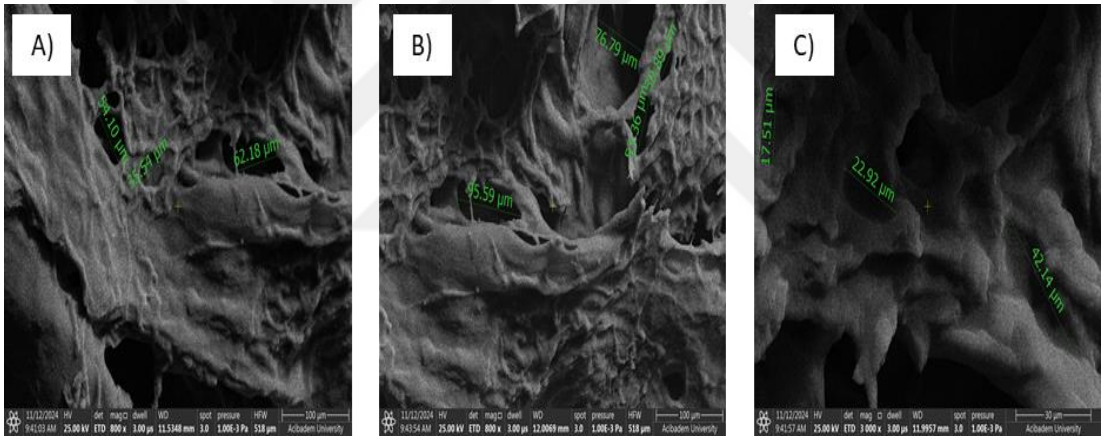

Figure 4.34 Morphological Imaging of Ch-PEG5k-PEGDGE20-HA1-CA (HG24) hydrogel (magnification: A-800x, B-800x, C-3000x)

Hydrogels formed by adding carvacrol to the HG19 structure were subjected to morphological analysis with SEM device after lyophilization. Figure 4.34 (A, B and C) show the porous structure, pore sizes and interconnectivity of the hydrogel network, which is critical for drug encapsulation and release efficiency. These hydrogels, designated as H24, showed porous structures between 30-100 µm at 800x magnification, while small pores of 17 or 22 µm were observed at higher magnifications such as 3000x.

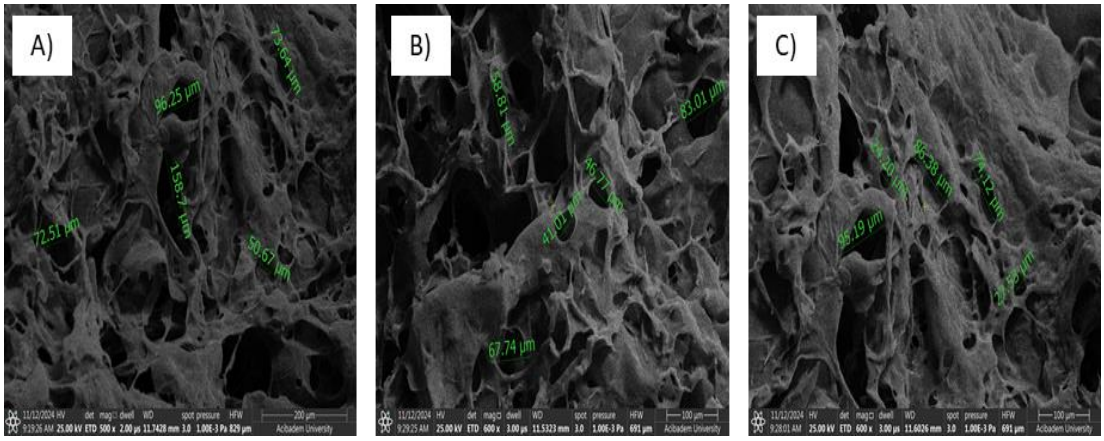

Figure 4.35 Morphological Imaging of Ch-PEG5k-PEGDGE20-AV2-CA (HG25) hydrogel (magnification: A-500x, B-600x, C- 600x)

Hydrogels formed by adding carvacrol to the HG22 structure were subjected to morphological analysis with SEM device after lyophilization. Figure 4.35 (A, B and C) show the porous structure, pore sizes and interconnectivity of the hydrogel network, which is critical for drug encapsulation and release efficiency. These hydrogels, designated as H24, showed porous structures between 40-150 µm at 500x and 600x magnification.

4.4.4 Drug Release Profile

4.4.4.1 Calibration Curve for Carvacrol

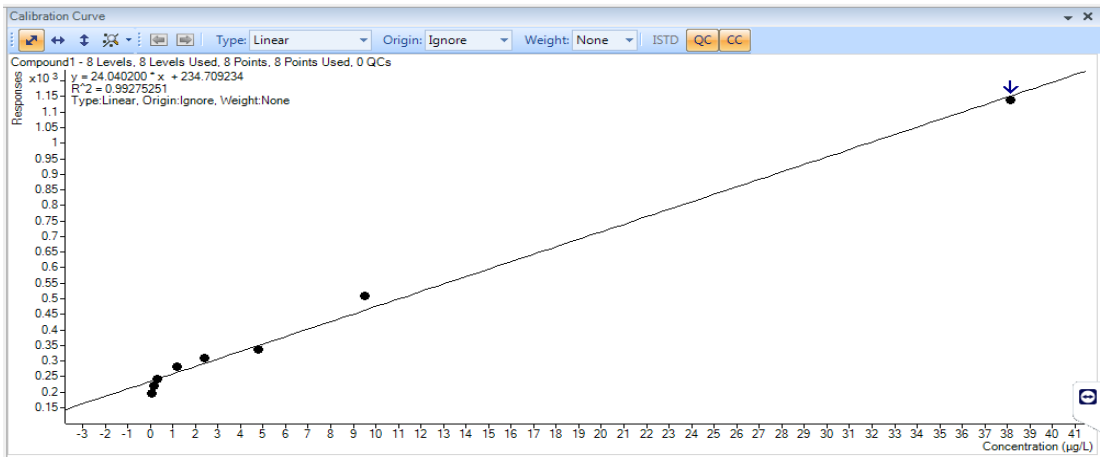

Figure 4.36 Calibration curve of carvacrol

Hydrogels prepared in this study were enhanced by the therapeutic effect of carvacrol molecules for their ability to reduce the inflammation at the wound area and ameliorating role in wound healing. Encapsulated carvacrol molecules were expected to release in physiological environments, preferably faster in inflammatory area. In order to calculate how much of the loaded drug is released from the hydrogel system, LC-MS/MS instrument was utilized. A method specific to the molecular ion of carvacrol was determined in this instrument and standard samples prepared by pure carvacrol were run with this method. Figure 4.36 shows the obtained calibration curve for carvacrol, which covers the concentration range in ppm.

4.4.4.2 Drug Release Profile

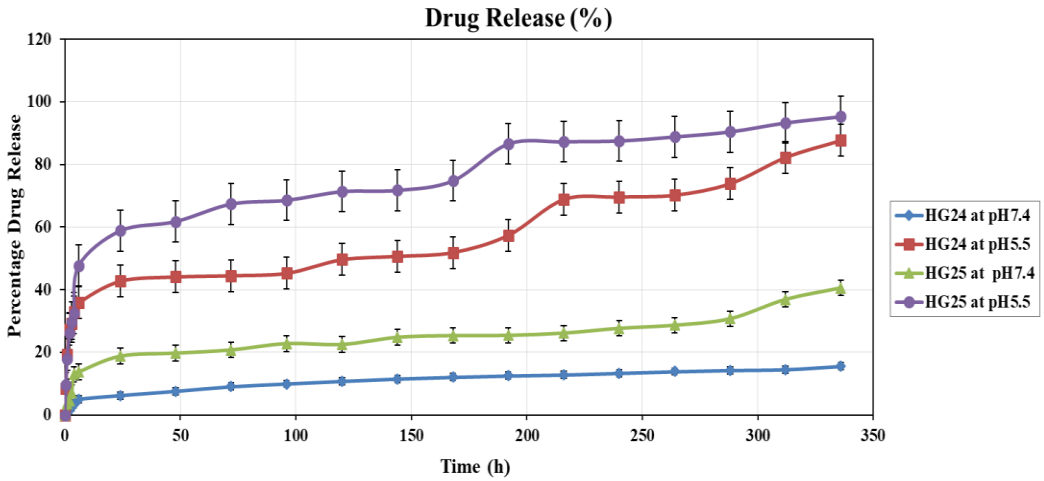

Figure 4.37 Drug release kinetics of HG24 (Ch-PEG5k-PEGDGE20-HA1-CA) and HG25 (Ch-PEG5k-PEGDGE20-AV2-CA) at different pH levels

The drug release profiles for HG24 and HG25 in Acetate Buffer (pH 5.5) and PBS (pH 7.4) solutions were determined at body temperature (37 °C) in neural (pH: 7.4) and slightly acidic (pH: 5.5) environment for 14 days. The hydrogels were placed in dialysis membranes with a molecular cut-off value 1kDa, and the receptor solutions used were 10 mM pH: 7.4 PBS solution as neutral environment to represent the healthy physiological conditions and acetate buffer that represent acidic environment with pH 5.5, which is mostly seen in inflammated tissues upon wound healing process. These

receptor solutions were used as 40 mL, which was at least 10 times higher than the solubility of carvacrol in water. So these conditions fulfil the need for ‘sink’ conditions that was required for the release studies of hydrophobic drug molecules. These dialysis set-ups were incubated at 37 °C in an orbital shaker for the simulation of body conditions. The samples collected at different time points from the receptor solutions were stored at -20 °C for further analysis.

Amount of free drug molecules in the collected samples were determined by using LC-MS/MS instrument. Each sample was run through an C18 column and the mobile phase contained 50% ACN and 50% H_2O with a flow rate of 0.5mL/min. Obtained data was evaluated and compared based on the calibration curve prepared specifically for carvacrol molecules. Drug release profiles demonstrated in Figure X indicates a slower release of carvacrol in pH7.4 compared to acidic environment. HG24 (with HA) in PBS solution showed the lowest drug release, reaching a maximum release of 15%, whereas HG25 hydrogel (with AV) showed higher release, reaching around 40% release. In addition, HG24 in acetate buffer reached a maximum of about 90%, and HG25 hydrogels reached a maximum release of 95% in acidic environment. Therefore, it can be concluded that hydrogels including AV showed a faster release compared to the ones with HA.

5 DISCUSSION

Skin is the largest organ in human. It supports defence against bacterial or viral infection and tissue dehydration and maintain body temperature. However, it can be easily damaged by external forces and diseases like diabetes ulcers. Since ancient times, people have been experimenting with ways to solve this disease. These include negative pressure Wound Therapy (NPWT), hyperbaric oxygen Therapy, and debridement, a type of surgery. However, there is still no complete solution. The hydrogel design realized within the scope of the thesis is aimed at being an alternative solution from natural source to this problem.

In this context, first, mPEG molecules of different weights were converted into PEG-COOH by reaction with succinic anhydride. Thus, the chemical structure of the PEG molecule was changed and made more suitable for chemical binding. Then, chitosan and PEG-carboxylic acid molecules were conjugated. Thus, a hybrid structure was obtained by linking one natural and one synthetic molecule. The chemical structure of the conjugate was analyzed by FT-IR and NMR spectroscopies. As a result of the analysis, bond structures from chitosan and PEG structures were observed in the conjugate structure. (61, 62)

In the next step, the optimal working environment of the cross linker was analysed. For the optimal working ratio of the PEGDGE cross linker, different amounts of cross linker were added to the solutions at different temperatures and pH values. It was observed that the cross linker worked best in a neutral medium and in volume ratios. In the analysis at 65 and 80 °C temperature conditions, the chemical structure analysis was almost the same, but in the mechanic analysis, it was analysed that the hydrogels formed at 65 degrees were more durable. Hydrogels with bulk structure were obtained from conjugates formed from chitosan, chitosan, and PEG molecules of different weights through PEGDGE cross linker at the rates of 10, 20, and 40% by volume.

The conversion ratios of nine hydrogels were calculated, their chemical, morphological, and mechanical properties were analysed, and their water retention capacities were measured. When the conversions were compared, it was analysed that

the rate increased as the PEG weight in the Ch-PEG conjugate, which constitutes the main structure, increased, but no correlation was found with the increase in the amount of cross linker. Once the obtained FT-IR were compared. Overall, the FTIR analysis confirms that the hydrogels have the desired chemical structure, with the expected functional groups present in all samples. The spectra show consistent and well-defined peaks for O-H, C-H, C=O, and C-O stretching vibrations, indicating that the hydrogels were successfully synthesized with the intended chemical bonds. (63) Gels formed by adding different ratios of cross linker to chitosan, Ch-PEG2k (C1) and Ch-PEG5k (C2) conjugates, were subjected to mechanical analysis using a rheometer. As a result of these analyses, it was understood that gelation occurred in all joints. Initially, it was observed that the hydrogels formed from the conjugate had a higher G' value compared to the hydrogels formed from chitosan. As a result of these analyses, a linear relationship was generally observed between the PEG weight in the conjugate and the initial G' value. All hydrogels entered into the degradation process as a result of the increasing pressure effect. Ch-PEG5k (C2) conjugates were compared among themselves. Ch-PEG5k-PEGDGE10 (HG15) and Ch-PEG5k-PEGDGE40 (HG17) hydrogels lost their physical form at a certain point and entered into a rapid degradation process, but Ch-PEG5k-PEGDGE20 (HG16) gradually decreased and degraded more stably. Two of the nine hydrogels degraded the moment they came into contact with water and were not included in the analysis because they did not ensure the continuity of the experiment. Among the seven samples, the gels formed by adding different ratios of crosslinker to the Ch-PEG5k conjugate had lower swelling rates. Ideally, for controlled release systems, one prefers hydrogels that do not swell or only minimally (64) When Ch-PEG5k conjugate samples were compared among themselves, it was understood that the Ch-PEG5k-PEGDEGE40 (HG17) hydrogel swelled first, then degraded, and then swelled again. This means that the process of swelling and reaching the maximum saturation point and then entering the degradation process, which is the main feature of water holding capacity, is not as desired. Ch-PEG5k-PEGDEGE10 (HG15) and Ch-PEG5k-PEGDEGE20 (HG16) were realized as expected. In the comparison between Ch-PEG5k-PEGDEGE10 and Ch-PEG5k-PEGDEGE20 hydrogels, it was observed that the conversion of Ch-PEG5k-PEGDEGE10 hydrogels was higher. This value, which is above one hundred, is due to the incomplete drying of the hydrogel, and it is decided

that this hydrogel is not suitable for research. The microstructure of the hydrogel formed by crosslinking Ch-PEG5k conjugate with PEGDGE at 20% by volume is shown by SEM. These images show a large pore space in the crosslinked hydrogel. Such pores can affect the swelling capacity, water taking and molecular diffusion of the hydrogel. The fibrous and irregular structures represent the network structure formed by the action of the PEGDGE crosslinker. This network structure strengthens the mechanical properties of the hydrogel and stabilizes the porous structure. As a result, the variation of pore sizes suggests that it could be a qualified candidate for controlled drug delivery or some biomedicine applications in tissue engineering.

The first natural means of wound healing have been long sought after. Hyaluronic acid and Aloe Vera are some. Due to their chemical structure, they help the molecules in the wound-healing process. These materials were added to the hydrogels prepared within the scope of this thesis both to accelerate the healing process and to add structural strength. Among the nine hydrogels, the hydrogel formed by adding 20% by volume of cross linker to the Ch-PEG5k conjugate and named Ch-PEG5k-PEGDGE20 (HG16) was selected as the most optimal. HA and AV were added to this hydrogel at 0.5, 1 and 2% by weight. The conversion ratios and water uptake capacities of the six gels obtained with the added materials were calculated, and their chemical, physical, and morphological properties were analysed. When either hydrogels containing the same amount of HA or AV were compared, it was observed that the gels formed with the addition of HA had almost three times the conversion of the gels formed with the addition of AV. This means that the gels formed with HA have a more bulky structure and the molecules are more tightly bound to each other. In addition, no linear collinearity was found between the addition rate of the added material and the conversion. Chemical analysis of the six hydrogels formed showed that they contained the added materials (HA or AV) and the basic chemical structure (characteristic bands of PEGDGE and Ch-PEG5k). As the concentration of HA or AV increases, especially OH and C=O stress vibrations increase, confirming the contribution of the added material in the structure and supporting the cross-linking mechanism. (65, 66) The data presented by the graph reveals that hydrogels with low HA ratios lose elasticity faster and their structural integrity deteriorates, whereas high HA ratios provide a longer-lasting and durable

structure. On the other hand, the increase of C-O and Si-O vibrations in particular indicates that Aloe Vera incorporates biological functional groups into the structure, which means that it can increase the properties of the hydrogel, such as biocompatibility and wound healing. Hydrogels formed by adding AV and HA to the hydrogel named as Ch-PEG5k-PEGDGE20 (HG16) were subjected to mechanical analysis. Figure 4.26 highlights the variation of G' and G" values between different HA concentrations (0.5, 1 and 2%). As seen in Figure 4.26-A, the G' values show a corresponding increase in elastic modulus as the HA concentration increases from 0.5% to 2%. This increase in G' value reflects a stiffer hydrogel network structure, which can be attributed to enhanced crosslinking facilitated by higher HA content. Conversely, Figure 4.26-B shows G" values representing the viscous or energy dissipative behaviour of the hydrogels. Similar to the G' trends, G" also increases with higher HA concentrations. However, the viscous response appears to be more pronounced at lower strains, indicating that the material becomes more elastic with higher HA content while retaining significant viscous behaviour under minimal stress. (67) This dual elastic-viscous property is crucial for mimicking the behaviour of biological tissues and provides the hydrogel with the necessary flexibility and resilience for wound healing applications. Figure 4.27 compares the elastic and viscous moduli of hydrogels (0.5, 1 and 2%) containing Aloe Vera (AV). In particular, the Ch-PEG5k-PEGDGE20-AV0.5 sample shows the highest G' values, indicating a stiffer network structure compared to the 1 and 2% AV samples. Interestingly, the 2% AV sample (Ch-PEG5k-PEGDGE20-AV2) shows a relatively lower elastic modulus, suggesting that higher concentrations of AV may interfere with the optimal crosslinking of the hydrogel, leading to reduced mechanical integrity. In addition, the viscous modulus (G") curves reveal that all formulations exhibit strong viscoelastic properties, but a trend of decreasing G" with increasing AV concentration is evident, indicating a decrease in the hydrogel's ability to dissipate energy under stress. (64) Hydrogels formed by adding different ratios of AV and HA by weight were measured using the aid method and calculated as percentages by formulation. In the graph shown in Figure 4.28, the swelling ratio showed an increasing trend with concentration due to the denser cross-linked network leading to higher water absorption capacity. However, the hydrogel with the highest percentage did not show a stable profile. These results indicate that the more stable profile Ch-PEG5k-PEGDGE-HA1

(HG19) hydrogel has favourable swelling ability and has the potential to be used as a wound dressing. Apart from that, Ch-PEG5k-PEGDGE-AV2 (HG23) has similar swelling features to it. The morphological characteristics analysed with the addition of other materials are presented in Figures 4.30 and 4.31. The density of the pore structure in the scaffold decreased with the addition of HA. Pore density refers to the average number of holes per inch of length. Since the pore size of the Ch-PEG5k scaffold was the largest, the conjugate had the minimum pore density. Ch-PEG5k (C2) scaffolds had the lowest porosity with the largest average pore size compared to HA hydrogels. HA is tightly combined with other materials due to its mechanical properties and reduces the surface pore density through electrostatic interaction. (68) On the other hand, the increase in AV concentration resulted in a higher pore density per unit area and a more uniform pore distribution. (69) As a result of the analysis, Ch-PEG5k-PEGDGE20-HA1 (HG19) was selected as the most optimal in terms of drug release profile in terms of porous structure, durability and water retention capacity among the three hydrogels formed by HA addition. Among the three hydrogels formed with the addition of AV, Ch-PEG5k-PEGDGE20-AV2 (HG23) was selected because it showed similar properties with Ch-PEG5k-PEGDGE20-HA1 (HG19).

Carvacrol, an extract from plants like thyme, is favoured for wound healing because of its anti-inflammatory, antioxidant, and antimicrobial properties. In this thesis, these materials were encapsulated in hydrogels. The conversion of the newly formed hydrogels was calculated, their chemical and morphological properties were analyzed, and the release profile at different pH values was investigated. Out of the two hydrogels formed, due to the bulk structure with HA inside, it had twice the conversion compared to the hydrogel with AV in it, similar to previous analyses. The chemical spectral changes in Figures 4.32 and 4.33 support the conclusion that carvacrol was effectively embedded into Ch-PEG5k-PEGDGE20-HA1 (HG19) and Ch-PEG5k-PEGDGE20-AV2 (HG23) hydrogels without losing its phenolic structure, thus enhancing the wound healing capacity of the hydrogel while retaining its potential bioactive properties. (70) In Figure 4.34, the pore structures are smaller and irregular. Pore sizes vary between 2-76 μm. While small pores provide advantages for controlled drug release and mechanical stability, fluid and cell diffusion may be limited. Due to the density of the

structure, this region seems to be more suitable for situations where slow drug release is required. (71) In figure 4.35, the pore structure shows a wider and more regular distribution. Pore sizes ranged between 42-158 μm, forming a large and connected network. These structures provide advantages in terms of high fluid retention capacity and cell infiltration. However, large pores can reduce mechanical strength and lead to faster drug release. (71) Figure 4.37, which measures the drug release of Ch-PEG5k-PEGDGE20-HA1 (HG19) and Ch-PEG5k-PEGDGE20-AV2 (HG23) hydrogels containing carvacrol (CA) at two pH levels (7.4 and 5.5), shows that at pH 5.5 both hydrogels exhibit significantly higher release profiles compared to those at pH 7.4. Comparing this data with previous studies, a similar trend is observed where drug release increases in more acidic environments. (72) This comparison emphasizes that the cross-linking density of the hydrogel and ionic interactions play important roles in modulating drug release rates depending on the environmental pH. Accelerated release at pH 7.4 is promising for applications in neutral pH environments such as skin or wound healing, while the highest release at acidic pH may be beneficial for prolonged drug delivery in environments such as infected tissues or tumours, which generally have lower pH. (73, 74) These results confirm the versatility of the hydrogel formulation for various therapeutic applications and support its potential as a controlled drug delivery system.

6 CONCLUSION

The presented study has investigated a novel chitosan-based hydrogel modified by conjugating to different molecular weights of PEG (2 and 5 kDa) for the efficient delivery of carvacrol for its sustained release in wound healing applications. Chemical, mechanical, and morphological analyses of the hydrogels showed that chitosan was effectively conjugated with PEG via crosslinking by PEGDGE, which allowed for the stabilization of a gel network with improved functionality. The introduction of Hyaluronic Acid and Aloe Vera strengthened the hydrogel structure, which can be adopted into potential dermal applications. The encapsulation of carvacrol into the hydrogel matrix provided a sustained release mechanism, which might thus efficiently augment its potential therapeutic effect on wound healing. According to these results, the hydrogel system developed in this study satisfies an intended goal for a biocompatible and mechanically stable drug delivery platform. This slow-release trend of carvacrol, complemented by the synergistic effects of natural components, seems to have a great potential for providing an attractive strategy for more effective wound coverage by preventing infections and stimulating tissue healing. Future work might pivot on tailoring the hydrogel composition depending on wound type and exploring the long-term stability of this system in vivo. The study serves as a first step in the further development of hydrogel-based drug delivery systems for skin with potential breakthroughs and has many implications for future advancements in treatment options.

7 REFERENCES

1. Leach JB, Bivens KA, Patrick CW Jr , CE S. Photocrosslinked hyaluronic acid hydrogels: natural, biodegradable tissue engineering scaffolds. Biotechnol Bioeng. 2003;82(5):578-89.
2. Lee SC, Kwon IK, Park K. Hydrogels for delivery of bioactive agents: a historical perspective. Adv Drug Deliv Rev. 2013;65(1):17-20.
3. Xinming L, Yingde C, Lloyd AW, Mikhalovsky SV, Sandeman SR, Howel CA, et al. Polymeric hydrogels for novel contact lens-based ophthalmic drug delivery systems: a review. Cont Lens Anterior Eye. 2008;31(2):57-64.
4. Yang Y, Xu L, Wang J, Meng Q, Zhong S, Gao Y, et al. Recent advances in polysaccharide-based self-healing hydrogels for biomedical applications. Carbohydr Polym. 2022;283:119161.
5. Cao J, Yuan P, Wu B, Liu Y, Hu C. Advances in the research and application of smart-responsive hydrogels in disease treatment. Gels. 2023;9(8).
6. Chatterjee S, Hui PC. Review of applications and future prospects of stimuli-responsive hydrogel based on thermo-responsive biopolymers in drug delivery systems. Polymers (Basel). 2021;13(13).
7. Hameed H, Faheem S, Paiva-Santos AC, Sarwar HS, Jamshaid M. Comprehensive review of hydrogel-based drug delivery systems: classification, properties, recent trends, and applications. AAPS PharmSciTech. 2024;25(4):64.
8. Hamidi E , Alhaloush R, Senol S, Akyol E. An overview on current trends and future outlook of hydrogels in drug delivery Sigma J Eng Nat Sci. 2023; Vol. 41:pp. 1047−61.
9. Jiang L, Gentile C, Lauto A, Cui C, Song Y, Romeo T, et al. Versatile fabrication approach of conductive hydrogels via copolymerization with vinyl monomers. ACS Appl Mater Interfaces. 2017;9(50):44124-33.
10. Ghanaatian E, Entezam M. Mechanical properties and drug release rate of poly(vinyl alcohol)/poly(ethylene glycol)/clay nanocomposite hydrogels: Correlation with structure and physical properties. Journal of Applied Polymer Science. 2019;136(32).
11. Sadat Shojai M, Khorasani MTJ, A. 3-Dimensional cell-laden nano-hydroxyapatite/protein hydrogels for bone regeneration applications. Materials Science and Engineering C 2015;49:835-43.
12. Wang M, Deng Z, Guo Y, Xu P. Engineering functional natural polymer-based nanocomposite hydrogels for wound healing. Nanoscale Adv. 2022;5(1):27-45.
13. Khan MUA, Aslam MA, Abdullah MFB, Al-Arjan WS, Stojanovic GM, Hasan A. Hydrogels: Classifications, fundamental properties, applications, and scopes in recent advances in tissue engineering and regenerative medicine – A comprehensive review. Arabian Journal of Chemistry. 2024;17(10).
14. Jacob S, Nair AB, Shah J, Sreeharsha N, Gupta S, Shinu P. Emerging role of hydrogels in drug delivery systems, tissue engineering and wound management. Pharmaceutics. 2021;13(3).
15. Sikdar P, Md. Uddin M , Dip T, Islam S, Hoque S, Dhar A, et al. Recent advances in the synthesis of smart hydrogels. Materials Advances. 2021.

16. Kim J, Lee K, Hefferan T, Currier B, Yaszemski M, Lu L. Synthesis and evaluation of novel biodegradable hydrogels based on poly(ethylene glycol) and sebacic acid as tissue engineering scaffolds. Biomacromolecules. 2007;9(1):149–57.
17. Germershaus O, Luhmann T, Rybak J, Ritzer J, Meinel L. Application of natural and semi-synthetic polymers for the delivery of sensitive drugs. International Materials Reviews. 2015;60.
18. Vicente D, Proenca DN, Morais PV. The role of bacterial polyhydroalkanoate (PHA) in a sustainable future: a review on the biological diversity. Int J Environ Res Public Health. 2023;20(4).
19. Gao L, Zha G, Wang Y, Lu Q, Zhu W, Shena Z, et al. Injectable drug-loaded hydrogel using "clickable" amphiphilic triblock copolymer as precursor. Polymer Chemistry. 2015(48):8240-3.
20. Chen SL, Fu RH, Liao SF, Liu SP, Lin SZ, Wang YC. A PEG-based hydrogel for effective wound care management. Cell Transplant. 2018;27(2):275-84.
21. Li J, Azizi A, Zhou S, Liu S, Han C, Chang Z, et al. Hydrogel polymer electrolytes toward better zinc-ion batteries: a comprehensive review. eScience. 2024.
22. Du X, Liu Y, Wang X, Yan H, Wang L, Qu L, et al. Injectable hydrogel composed of hydrophobically modified chitosan/oxidized-dextran for wound healing. Mater Sci Eng C Mater Biol Appl. 2019;104:109930.
23. Gounden V, Singh M. Hydrogels and Wound Healing: Current and Future Prospects. Gels. 2024;10(1).
24. Ishihara M, Ono K, Sato M, Nakanishi K, Saito Y, Yura H, et al. Acceleration of wound contraction and healing with a photocrosslinkable chitosan hydrogel. Wound Repair Regen. 2001;9(6):513-21.
25. Loo HL, Goh BH, Lee LH, Chuah LH. Application of chitosan-based nanoparticles in skin wound healing. Asian J Pharm Sci. 2022;17(3):299-332.
26. Golmohammadi R, Najar-Peerayeh S, Tohidi Moghadam T, Hosseini SMJ. Synergistic antibacterial activity and wound Healing properties of selenium-chitosan-mupirocin nanohybrid system: an in vivo study on rat diabetic staphylococcus aureus wound infection model. Sci Rep. 2020;10(1):2854.
27. Hao Y, Zhao W, Zhang H, Zheng W, Zhou Q. Carboxymethyl chitosan-based hydrogels containing fibroblast growth factors for triggering diabetic wound healing. Carbohydr Polym. 2022;287:119336.
28. Sudhakar K, Ji SM, Kummara MR, Han SS. Recent Progress on Hyaluronan-Based Products for Wound Healing Applications. Pharmaceutics. 2022;14(10).
29. Pecova J, Rohlikova V, Smoldasova M, Marek J. Clinical efficacy of hyaluronic acid with Iodine in hard-to-heal wounds. Pharmaceutics. 2023;15(9).
30. Ramos-Torrecillas J, Garcia-Martinez O, De Luna-Bertos E, Ocana-Peinado FM aRC. Effectiveness of platelet-rich plasma and hyaluronic acid for the treatment and care of pressure ulcers. Biol Res Nurs. 2015;17(2):152-8.
31. Kazkayası I, Denizaltı M. The effects of metformin and hyaluronic acid on wound healing in high glucose incubated fibroblast cells. Marmara Pharmaceutical Journal. 2023(27(4)):1338-45.

32. Humbert P, Mikosinki J, Benchikhi H, Allaert FA. Efficacy and safety of a gauze pad containing hyaluronic acid in treatment of leg ulcers of venous or mixed origin: a double-blind, randomised, controlled trial. Int Wound J. 2013;10(2):159-66.
33. Tariq M, Tahir HM, Butt SA, Ali S, Ahmad AB, Raza C, et al. Silk derived formulations for accelerated wound healing in diabetic mice. PeerJ. 2021;9:e10232.
34. Sidiq F. Review of the healing potential of burn wounds with aloe vera extract cream: the influence of formula and virgin coconut oil application. International Journal of Health, Medicine, and Sports. 2023;1 (4):20-4.
35. Mohi-Eldin MM, Allaam AA. Clinical and Pathological Assessment of Aloe Vera and Propolis for Wound Healing in Normal and Diabetic Albino Rats. Zagazig Veterinary Journal. 2017;45:314-25.
36. Tarameshloo M, Norouzian M, Zarein-Dolab S, Dadpay M, Mohsenifar J, Gazor R. Aloe vera gel and thyroid hormone cream may improve wound healing in Wistar rats. Anat Cell Biol. 2012;45(3):170-7.
37. Sarkhil M, Prakash K, Haseeb A, Ahmed K, Udupa P, Muguregowda H. Evaluation of altered ground matrix and matrix metalloproeinase (MMP'S) in wound healing with Aloe vera extract. Asian Journal of Pharmacy and Pharmacology. 2020;6(1):32-6.
38. Carvalho Lima EN, Barros Martins G, Diaz R, Schechter M, Piqueira J, Justo J. Effects of carbon nanomaterials and aloe vera on melanomas-where are we? recent updates. Pharmaceutics. 2022;14(10).
39. Thang NH, Chien T, Cuong D. Polymer-Based Hydrogels Applied in Drug Delivery: An Overview. Gels. 2023;9(7).
40. Zhang W, Liu, L., Cheng, H, Zhu, J, Li, X, Ye, S and Li, X. Hydrogel-based dressings designed to facilitate wound healing. Materials Advances. 2023;5.
41. Deptula M, Zawrzykraj M, Sawicka J, Banach-Kopec A, Tylingo R, Pikula M. Application of 3D-printed hydrogels in wound healing and regenerative medicine. Biomed Pharmacother. 2023;167:115416.
42. Bhaladhare S, Das D. Cellulose: a fascinating biopolymer for hydrogel synthesis. Journal of Materials Chemistry B. 2022;10(12):1923-45.
43. Vo TN, Ekenseair AK, Kasper FK, Mikos AG. Synthesis, physicochemical characterization, and cytocompatibility of bioresorbable, dual-gelling injectable hydrogels. Biomacromolecules. 2014;15(1):132-42.
44. Gomes AR, Varela CL, Tavares-da-Silva EJ, Roleira FMF. Epoxide containing molecules: A good or a bad drug design approach. Eur J Med Chem. 2020;201:112327.
45. Lei Y, Liu L, Scholes CA, Kentish SE. Crosslinked PVA based polymer coatings with shear-thinning behaviour and ultralow hydrogen permeability to prevent hydrogen embrittlement. International Journal of Hydrogen Energy 2024;54:947-54.
46. Sung J, Lee, DG, Lee S, Park, J , Jung, HW. Crosslinking dynamics and gelation characteristics of photo- and thermally Polymerized poly(Ethylene Glycol) hydrogels. Materials. 2020;13.

47. Waters DJ, Engberg K, Parke-Houben R, Hartmann L, Ta CN, Toney MF, et al. Morphology of photopolymerized end-linked poly(ethylene glycol) hydrogels by small angle X-ray scattering. Macromolecules. 2010;43(16):6861-70.
48. Gaharwar AK, Peppas NA, Khademhosseini A. Nanocomposite hydrogels for biomedical application. Biotechnol Bioeng. 2014;111(3):441-53
49. Monticelli D, Martina V, Mocchi R, Rauso R, Zerbinati U, Cipolla G, et al. Chemical characterization of hydrogels crosslinked with polyethylene glycol for soft tissue augmentation. Open Access Maced J Med Sci. 2019;7(7):1077-81.
50. Kim DH, Han JH, Kwon HC, Lim SJ, Han SG, Jung HS, et al. Toxicity assessment of a single dose of poly(ethylene glycol) diglycidyl ether (PEGDE) administered subcutaneously in mice. Toxics. 2021;9(12).
51. Liu M, Jin J, Zhong X, Liu, L, Tang, C, Cai, L. Polysaccharide hydrogels for skin wound healing. Heliyon. 2024;10(15).
52. Kim K, Siddiqui Z, Acevedo-Jake AM, Roy A, Choudhury M, Grasman J, et al. Angiogenic hydrogels to accelerate early wound healing. Macromol Biosci. 2022;22(7):e2200067.
53. Imran M, Aslam M, Alsagaby SA, Saeed F, Ahmad I, Afzaal M, et al. Therapeutic application of carvacrol: A comprehensive review. Food Sci Nutr. 2022;10(11):3544-61.
54. Hotta M, Nakata R, Katsukawa M, Hori K, Takahashi S, Inoue H. Carvacrol, a component of thyme oil, activates PPARalpha and gamma and suppresses COX-2 expression. J Lipid Res. 2010;51(1):132-9.
55. Yan C, Kuang W, Jin L, Wang R, Niu L, Xie C, et al. Carvacrol protects mice against LPS-induced sepsis and attenuates inflammatory response in macrophages by modulating the ERK1/2 pathway. Sci Rep. 2023;13(1):12809.
56. Scaffaro R, Lopresti F, D'Arrigo M, Marino A, Nostro A. Efficacy of poly(lactic acid)/carvacrol electrospun membranes against Staphylococcus aureus and Candida albicans in single and mixed cultures. Appl Microbiol Biotechnol. 2018;102(9):4171-81.
57. Javed H, Meeran MFN, Jha N, Ojha S. Carvacrol, a Plant Metabolite Targeting Viral Protease (Mpro) and ACE2 in Host Cells Can Be a Possible Candidate for COVID-19. Frontiers in Plant Science. 2020;11.
58. Pan NC, Pereira HCB, da Silva MLC, Vasconcelos AFD, Celligoi M. Improvement Production of Hyaluronic Acid by Streptococcus zooepidemicus in Sugarcane Molasses. Appl Biochem Biotechnol. 2017;182(1):276-93.
59. Jithendra P, Rajam AM, Kalaivani T, Mandal AB, Rose C. Preparation and characterization of aloe vera blended collagen-chitosan composite scaffold for tissue engineering applications. ACS Appl Mater Interfaces. 2013;5(15):7291-8.
60. Marinelli L, Cacciatore I, Eusepi P, Di Biase G, Morroni G, Cirioni O, et al. Viscoelastic behaviour of hyaluronic acid formulations containing carvacrol prodrugs with antibacterial properties. Int J Pharm. 2020;582:119306.

61. Esmaeili Y, Dabiri A, Mashayekhi F, Rahimmanesh I, Bidram E, Karbasi S, et al. Smart co-delivery of plasmid DNA and doxorubicin using MCM-chitosan-PEG polymerization functionalized with MUC-1 aptamer against breast cancer. Biomed Pharmacother. 2024;173:116465.
62. Yari-Ilkhchi A, Ebrahimi-Kalan A, Farhoudi M, Mahkam M. Design of graphenic nanocomposites containing chitosan and polyethylene glycol for spinal cord injury improvement. RSC Adv. 2021;11(33):19992-20002.
63. Ali M, Mohamed MI, Taher AT, Mahmoud SH, Mostafa A, Sherbiny FF, et al. New potential anti-SARS-CoV-2 and anti-cancer therapies of chitosan derivatives and its nanoparticles: Preparation and characterization. Arab J Chem. 2023;16(5):104676.
64. Chelu M, Musuc AM, Aricov L, Ozon EA, Iosageanu A, Stefan LM, et al. Antibacterial Aloe vera Based Biocompatible Hydrogel for Use in Dermatological Applications. Int J Mol Sci. 2023;24(4).
65. Øvrebø Ø, Giorgi Z , De Lauretis A , Vanoli V , Castiglione F, Briatico-Vangosa F , et al. Characterisation and biocompatibility of crosslinked hyaluronic acid with BDDE and PEGDE for clinical applications. Reactive and Functional Polymers. 2024;200.
66. Sharma D, Singh B. Designing aloe vera-sterculia gum based copolymeric hydrogel dressings for drug delivery. Hybrid Advances. 2024;5.
67. Munar-Bestard M, Vargas-Alfredo N, Ramis J, Monjo M. Mangostanin hyaluronic acid hydrogel as an effective biocompatible alternative to chlorhexidine. International Journal of Biological Macromolecules. 2024;279.
68. Cheng R, Cao Y, Yan Y, Shen Z, Zhao Y, Zhang Y, et al. Fabrication and characterization of chitosan-based composite scaffolds for neural tissue engineering. International Journal of Polymeric Materials and Polymeric Biomaterials. 2021.
69. Wang Y, Zhang Y, Yang YP, Jin M, Huang S, Zhuang Z, et al. Versatile dopamine-functionalized hyaluronic acid-recombinant human collagen hydrogel promoting diabetic wound healing via inflammation control and vascularization tissue regeneration. Bioactive Materials. 2024;35.
70. Fratini C, Weaver E, Moroni S, Irwin R, Dallal Bashi YH, Uddin S, et al. Combining microfluidics and coaxial 3D-bioprinting for the manufacturing of diabetic wound healing dressings. Biomater Adv. 2023;153:213557.
71. Udenni Gunathilake TMS, Ching YC, Ching KY, Chuah CH, Abdullah LC. Biomedical and Microbiological Applications of Bio-Based Porous Materials: A Review. Polymers (Basel). 2017;9(5).
72. Keawchaoon L, Yoksan R. Preparation, characterization and in vitro release study of carvacrol-loaded chitosan nanoparticles. Colloids Surf B Biointerfaces. 2011;84(1):163-71.
73. Qu Z, Wang Y, Dong Y, Li X, Hao L, Sun L, et al. Intelligent electrospinning nanofibrous membranes for monitoring and promotion of the wound healing. Mater Today Bio. 2024;26:101093.
74. Zhang S, Ge G, Qin Y, Li W, Dong J, Mei J, et al. Recent advances in responsive hydrogels for diabetic wound healing. Materials Today Bio. 2023;18.

8 CURRICULUM VITAE